# Tumor-infiltrating macrophage associated lncRNA signature in cutaneous melanoma: implications for diagnosis, prognosis, and immunotherapy

**Qi Wan[1,*], Yuhua Deng[2,*], Ran Wei[1], Ke Ma[1], Jing Tang[1], Ying-Ping Deng[1]**

[1]Department of Ophthalmology, West China Hospital of Sichuan University, Chengdu, Sichuan, China
[2]Department of Infection Control, West China Hospital of Sichuan University, Chengdu, Sichuan, China
[*]Equal contribution and co-first authors

**Correspondence to:** Jing Tang, Ke Ma; **email:** tangjing0802@163.com, https://orcid.org/0000-0003-0720-8616; 280463919@qq.com, https://orcid.org/0000-0002-5193-428X

## ABSTRACT

**Along with the increasing knowledge of long noncoding RNA, the interaction between the long noncoding RNA (lncRNA) and tumor immune infiltration is increasingly valued. However, there is a lack of understanding of correlation between regulation of specific lncRNAs and tumor-infiltrating macrophages within melanoma. In this research, a macrophage associated lncRNA signature was identified by multiple machine learning algorithms and the robust and effectiveness of signature also validated in other independent datasets. The signature contained six specific lncRNAs (PART1, LINC00968, LINC00954, LINC00944, LINC00518 and C20orf197) was constructed, which could diagnose melanoma and predict the prognosis of patients. Moreover, our signature achieves higher accuracy than the previous well-established markers and regarded as an independent prognostic indicator. The pathway enrichment revealed that these lncRNAs were closely correlated with many immune processes. In addition, the signature was associated with different immune microenvironment and applied to predict response of immune checkpoint inhibitor therapy (low risk of patients well respond to anti-PD-1 therapy and high risk is insensitive to anti-CTLA-4 therapy). Therefore, our finding supplies a more accuracy and effective lncRNA signature for tumor-infiltrating macrophages targeting treatment approaches and affords a new clinical application for predicting the response of immunotherapies in melanomas.**

## INTRODUCTION

Malignant melanoma is the most dangerous skin cancer, which originates from melanocytes and possesses a larger proportion of metastases and death [1]. Recent evidence has shown that tumor microenvironment plays a critical role in formation and development of melanoma [2, 3]. Various infiltrating immune cells positively or negatively regulate tumor cell behaviors and finally result in tumor growth and metastasis [4]. Of particular interest, macrophages work as a major component of infiltrating immune cells, which participate to a large degree in melanoma cells' proliferation, metastasis and resistance to anticancer therapies [5, 6]. They can secrete growth factors, such as vascular endothelial growth factor (VEGF) and epidermal growth factor (EGF), which stimulate tumor angiogenesis and facilitate metastatic spread. Tumor associated macrophages (TAMs) also produce matrix metalloproteinases (MMPs) that degrade extracellular matrix components, allowing melanoma cells to invade surrounding tissues and form distant metastases [7, 8]. Furthermore, TAMs play a critical role in suppressing the anti-tumor immune response. They can inhibit the

activation and function of cytotoxic T cells, natural killer cells, and dendritic cells, thereby dampening the immune system's ability to recognize and eliminate melanoma cells. This immunosuppressive function of TAMs is mediated by the secretion of immunosuppressive cytokines, such as interleukin-10 (IL-10) and transforming growth factor-beta (TGF-β) [9, 10]. Hence, TAMs have been proven as an important therapeutic target to improve the efficacy of immunotherapy.

According to research on mammalian transcriptomes, protein-coding genes account for just 1.5 percent of the human genome. While around 70% of the overall human genome is continually producing a broad array of non-coding RNAs (ncRNAs), which are classified as small ncRNAs (200 nt) and long ncRNAs (lncRNAs, >200 nt) based on transcript length. Increasing evidence suggests that lncRNAs are involved in a wide range of biological activities, including cell proliferation, differentiation, migration, invasion, and death [11–14]. It has been proven that abnormal expression of lncRNAs plays essential jobs in carcinogenesis, such as gastric cancer, prostate cancer, and leukemia [15]. Moreover, previous studies suggested that lncRNAs widely regulated immune reactions such as antigen presentation or release, immune cell activation or infiltration. For instance, Elling et al. demonstrated that lincRNA-COX2 can directly regulate immune response by activating or inhibiting a class of immune genes [16]. Song et al. recently revealed that the NF-κB interacting lncRNA (NKILA) can activate inflammatory responses in the tumor microenvironment. Low NKILA expression has been linked to a poor prognosis of breast cancer [17]. Besides, Krawczyk et al. indicated that P50-associated cyclooxygenase-2 extragenic RNA (PACER) takes a crucial factor in the differentiation of macrophages [18]. Although lncRNAs emerge as a hot research topic in many aspects including cancer immunology, few numbers of macrophage associated lncRNAs have been investigated so far, and a new prognostic macrophage associated lncRNAs signature is needed continue to surprise us.

Therefore, in this research, we identified macrophage-associated lncRNAs from the ImmLnc database and then thoroughly analyzed the differentially expressed macrophage associated lncRNAs between tumor and normal in multiple public datasets. Next, we developed a macrophage lncRNA signature by integrating immune-related lncRNAs and clinical outcomes. We discovered that the expression of macrophage associated lncRNAs signature takes a crucial role in the prognosis of melanoma and displays more effective performance for prediction of immunotherapy response in melanoma patients.

## MATERIALS AND METHODS

### Macrophage associated lncRNA in melanoma

In TIMER2.0 website (http://timer.comp-genomics.org/), we astonished observed that tumor infiltrated macrophage cells were regarded as a prognostic factor and intimately associated with BRAF mutant in cutaneous melanoma patients (Supplementary Figure 1). Thus, the 3346 macrophage associated lncRNAs in cutaneous melanoma (Supplementary Table 1) were retrieved from the ImmLnc database (http://bio-bigdata.hrbmu.edu.cn/ImmLnc), which affords tools to explore the immune associated function of lncRNAs such as the correlation between lncRNA and immune cell types, lncRNA and pathways and cancer related lncRNAs across 33 types of cancer [19].

### Melanomas collection and normal controls

The TCGA-SKCM dataset (https://portal.gdc.cancer.gov) was used to obtain the lncRNAs expression and clinical variables of cutaneous melanoma, and the normal healthy skin tissue samples were obtained from the Genotype-Tissue Expression website (GTEx) (https://www.gtexportal.org/) to match the tumor samples. TPMs values were utilized to describe the expression level of lncRNAs for TCGA-SKCM & GTEx. Five independent melanoma patient datasets were acquired from GEO database for outside verification, which including GSE65904, GSE15605, GSE78220 (Hugo et al. study) [20] and GSE91061 (Riaz et al. study) [21]. Furthermore, to predict immunotherapy response, A prior cohort managed with CTLA-4 and PD-1 inhibitors was obtained from a previously published study [22]. The transcriptome profiles (FPKM) of these datasets were processed by applying their corresponding platform and was transformed into TPMs. Firstly, probes were annotated based on the annotation profile supplied by the platform, and non-matched probes were removed. If several probes were mapped to the same gene, the average value would be used to reflect gene expression. Variations in lncRNAs with low expression levels (TPMs <0.01) will then be eliminated due to their low expression level. Finally, the raw data were $log2(× + 1)$ transformed and quantile normalized. Figure 1 depicts a simplified procedure for the current investigation.

### Differential expression analysis of macrophage associated lncRNAs (DEMlncRNAs)

To explore the differentially expressed lncRNAs, samples in TCGA-SKCM & GTEx dataset were divided into melanoma and normal skin groups. The differentially expressed analysis of lncRNAs between

melanoma and normal skin was conducted by using 'limma package' in R software [23]. The cutoff criterion was the absolute value of log 2-fold change (FC) ≥2 and $p$-values < 0.05. Besides, the overlapping lncRNAs in differentially expressed lncRNAs and macrophage associated lncRNAs were defined as DEMlncRNAs.

## Development of DEMlncRNAs signature using machine learning

To identify the survival-related DEMlncRNAs in melanomas, we randomly categorized the melanoma patients in TCGA-SKCM dataset into train or validation samples with a ratio of 7:3. The survival associated DEMlncRNAs were then selected by using univariate Cox regression methodology in train dataset ($p$-values < 0.05). Next, multiple machine learnings contained Least Absolute Shrinkage and Selection Operator (LASSO), Random Forests Variable Selection (RF-VS), and Support Vector Machine-Recursive Feature Elimination (SVM-RFE) were applied to identify the essential DEMlncRNAs in the training dataset. LASSO screened the important features based on the misclassification error, SVM-RFE identified key factors by 5-fold cross-validation errors and RF-VS picked out significant variables by out of bag (OOB) error [24]. The common important DEMlncRNAs were selected out for further analysis. Firstly, the diagnostic model was built by neural network algorithm with these identified DEMlncRNAs. To assess the model's efficiency, the

confusion matrix and Receiver operating characteristic curves (ROC) were utilized. The prognostic risk model was then built using multivariate Cox regression analysis. The following is how the risk score is calculated:

$$\text{Risk score} = \sum_{i=1}^{N} (coef_i \times expr_i),$$

where $expr_i$ means the DEMlncRNA's relative expression in the risk model, $coef_i$ is stand for the DEMlncRNA's Cox coefficient, and N represents the number of DEMlncRNA. In the train set, the median value was used as a threshold for the DEMlncRNA signature risk score, and samples were divided into high- and low-risk categories. Kaplan-Meier survival curves and log-rank tests were used to compare the prognoses of the high- and low-risk groups. ROC curves and area under the curve (AUC) measurements were also used to evaluate the model's 3- and 5-year overall survival prediction accuracy. Furthermore, these DEMlncRNAs signatures were verified in the testing dataset and GSE65904 to establish the robustness of the conclusion.

## Pathway enrichment analysis

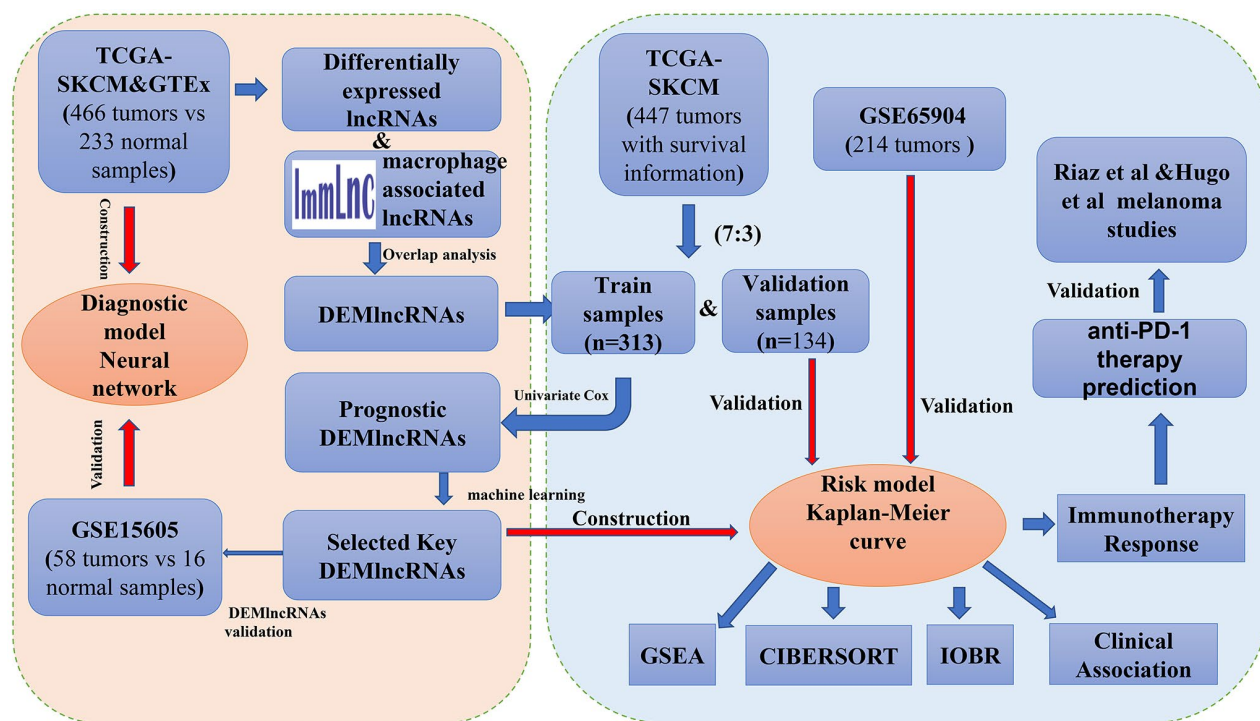To investigate the possible involvement of protein-coding genes co-expressed with DEMlncRNAs, the ENCORI website (http://starbase.sysu.edu.cn/index.php) was used.



Figure 1. The complete workflow of the analysis in this present study.

Second, Metascape (http://metascape.org) was utilized to perform functional enrichment of BP and the KEGG terms. In addition, immune-related pathways of DEMlncRNAs were examined in the ImmLnc database (http://bio-bigdata.hrbmu.edu.cn/ImmLnc). Pathways with $p$-value and adjust $p$-value < 0.05 were screened out and regarded as significance.

**Associations between risk score and other prognostic markers**

To calculate the relationships between risk score and other prognostic biomarkers, the correlation of risk score with traditional markers (age, clark level, stage.) and previously established prognostic markers included transcriptomic classification (named "immune", "keratin" and "MITF-low"), mutation subtype (named "BRAF subtype", "RAS subtype", "NF1 subtype" and "Triple Wild-Type subtype") and BRAF mutant were performed [25, 26]. Moreover, uni- and multi-variate Cox regression were performed in three datasets to analyze the prognostic significance of the risk score and traditional clinical factors to evaluate if the risk score is an independent prognostic factor. Next, to explore the association between risk score and immunological microenvironment, the Immuno-Oncology Biological Research (IOBR) approach was used. The CIBERSORT method was initially used to determine the relative proportions of 22 different kinds of infiltrated immune cells in each patient. Only immune cells have 50% value and patients with $P < 0.05$ were considered eligible for further analysis. Afterwards, previous user-built signatures associated with immune microenvironment were evaluated by ssGSEA, Principal Component Analysis (PCA), and Z-score methods. Finally, the associations for risk score with immune cell infiltration and immune-associated markers were studied further.

**Statistical analysis**

Every statistical analyses were carried out by R (version 3.6.0) or Python (version 3.8.0) and installed packages. The "glmnet" package performed the LASSO analysis. The "e1017" package was used to carry out the SVM-RFE approach. The "varSelRF" package was applied to the RF-VS algorithm. The "CIBERSORT" program estimated the CIBERSORT deconvolution. The "survival" and "survivalROC" packages were used to perform Kaplan-Meier (KM) survival analyses. The "IOBR" package estimated the IOBR algorithm. Python's "sklearn" module was used to run the neural network method. The Spearman algorithm was used to evaluate the correlation test. When comparing two groups, a Wilcoxon test was employed; when comparing more than two groups, Kruskal-Wallis tests

was utilized. To investigate the relationship between subgroup and clinicopathological variables, a Chi-square test was performed. The Cox regression analysis yielded hazard ratios (HR) and 95 percent confidence intervals (CI). In all tests, $P < 0.05$ was used to denote statistical significance.

**Availability of data and materials**

The datasets used and analyzed during the current study are available from the corresponding author on reasonable request.

# RESULTS

**Differentially expressed lncRNA in melanoma**

The normalized matrix data of lncRNA for cutaneous melanoma and normal samples (not sun exposed) were obtained from the TCGA-SKCM & GTEx, which included 466 melanomas and 233 normal samples. According to the selection criterion, 1640 differentially expressed lncRNAs were screened out in TCGA-SKCM & GTEx dataset, where 650 lncRNAs were significant up-regulation and 990 lncRNAs were significant down-regulation (Supplementary Figure 2A).

**Identification of validation of prognostic DEMlncRNAs signature**

According the results of overlap in macrophage associated lncRNAs and differentially expressed lncRNAs (Supplementary Figure 2B), 447 DEMlncRNAs were selected for further analysis (Supplementary Table 2). The heatmap of 447 DEMlncRNAs was shown in Supplementary Figure 2C. After excluding the patients without survival information, the TCGA-SKCM dataset were randomly separated into two independent datasets: train samples ($n = 313$) and validation samples ($n = 134$). Comparison of the clinical information between train and validation samples, no statistically significant differences were observed in two datasets (Table 1). Next, the relationships between 447 DEMlncRNAs and overall survival time in train sample were assessed by univariate Cox regression analysis, and we discovered 115 DEMlncRNAs were significantly correlated with survival (Figure 2A). In order to find the optimum signatures, machine learning methods were firstly performed to screen out the most important DEMlncRNAs in the train dataset. Combined the feature selection results from LASSO algorithm (Figure 2B), RF-VS algorithm (Figure 2C) and SVM-RFE algorithm (Figure 2D), we observed that six overlapping DEMlncRNAs were shared in these machine learning methods (Figure 2E and Supplementary Table 3).

**Table 1. Clinical characteristics of train and validation dataset.**

| | Level | Train samples | Validation samples | *P*-value |
|---|---|---|---|---|
| *n* | | 313 | 134 | |
| Overall survival time (median (IQR)) | | 3.02 (1.29, 6.48) | 3.03 (1.44, 6.26) | 0.823 |
| Age (median (IQR)) | | 59.00 (49.00, 72.00) | 57.00 (46.00, 68.75) | 0.115 |
| Gender (%) | Female | 118 (37.7) | 53 (39.6) | 0.793 |
| | Male | 195 (62.3) | 81 (60.4) | |
| Race (%) | Asian | 8 (2.6) | 4 (3.0) | 0.967 |
| | Not reported | 7 (2.2) | 3 (2.2) | |
| | White | 298 (95.2) | 127 (94.8) | |
| Melanoma clark level value (%) | | 97 (31.0) | 42 (31.3) | 0.780 |
| | I | 1 (0.3) | 0 (0.0) | |
| | II | 10 (3.2) | 8 (6.0) | |
| | III | 55 (17.6) | 21 (15.7) | |
| | IV | 116 (37.1) | 48 (35.8) | |
| | V | 34 (10.9) | 15 (11.2) | |
| Pathologic_M (%) | | 20 (6.4) | 6 (4.5) | 0.473 |
| | M0 | 275 (87.9) | 123 (91.8) | |
| | M1 | 18 (5.8) | 5 (3.7) | |
| Pathologic_N (%) | | 17 (5.4) | 2 (1.5) | 0.151 |
| | N0-1 | 225 (71.9) | 103 (76.9) | |
| | N2-3 | 71 (22.7) | 29 (21.6) | |
| Pathologic_T (%) | | 21 (6.7) | 6 (4.5) | 0.634 |
| | T0-1 | 77 (24.6) | 32 (23.9) | |
| | T2-4 | 215 (68.7) | 96 (71.6) | |
| Tumor stage (%) | I/II nos | 4 (1.3) | 6 (4.5) | 0.367 |
| | Not reported | 26 (8.3) | 10 (7.5) | |
| | Stage I | 51 (16.3) | 25 (18.7) | |
| | Stage II | 97 (31.0) | 41 (30.6) | |
| | Stage III | 118 (37.7) | 47 (35.1) | |
| | Stage IV | 17 (5.4) | 5 (3.7) | |
| Tumor status (%) | | 121 (38.7) | 50 (37.3) | 0.851 |
| | Tumor free | 122 (39.0) | 56 (41.8) | |
| | With tumor | 70 (22.4) | 28 (20.9) | |
| Radiation therapy (%) | | 123 (39.3) | 49 (36.6) | 0.275 |
| | No | 169 (54.0) | 70 (52.2) | |
| | Yes | 21 (6.7) | 15 (11.2) | |
| Vital status (%) | Alive | 169 (54.0) | 65 (48.5) | 0.190 |
| | Dead | 144 (46.0) | 68 (50.7) | |
| | Not reported | 0 (0.0) | 1 (0.7) | |
| Sample tissue (%) | Metastatic | 246 (78.6) | 100 (74.6) | 0.426 |
| | Primary tumor | 67 (21.4) | 34 (25.4) | |

Abbreviations: IQR: interquartile range; OS: overall survival.

Further comparison analysis between 58 melanomas and 16 normal skin samples in the GSE15605 dataset showed that five overlapping DEMlncRNAs had significant differences (Figure 2F). Furthermore, we used neural network algorithm to well establish a diagnostic model with six DEMlncRNAs in TCGA-SKCM & GTEx dataset (randomly split into train and test dataset with ratio = 7:3), which suggested good

accuracies and AUC values in train dataset (accuracy = 0.99 and AUC = 0.99) (Figure 3A, 3D) and test dataset (accuracy = 0.99 and AUC = 1.00) (Figure 3B, 3E). Even in GSE15605 dataset, our diagnostic model still revealed an excellent performance to distinguish normal and tumor patients with accuracy = 0.85 and AUC = 0.93 (Figure 3C, 3F).

Afterwards, the six DEMlncRNAs were subsequently performed to develop a risk model in train dataset by applying multivariate Cox analysis. Each patient's risk score was finally computed using the risk score formula. The risk model consisted of risk scores distribution, vital status, overall survival (OS) time, and heat map of DEMlncRNAs expression, which respectively illustrated in train (Supplementary Figure 3A),

validation (Supplementary Figure 3B) and GSE65904 (Supplementary Figure 3C) datasets. Next, we divided the melanoma patients in the train dataset into high-risk and low-risk groups based on the median value of the risk score. With a significant log-rank test of $p < 0.001$, the KM survival curves revealed that patients of high-risk group had substantially worse survival than low-risk group (Figure 4A). The ROC curve was drawn to estimate the ability of prediction power, and the AUCs of the curves were 0.619 at 3-year and 0.676 at 5-year respectively (Figure 4B). Moreover, to confirm the robustness of the six DEMlncRNAs based model, it was further verified in validation and GSE65904 datasets via the same cutoff value. The patients in validation and GSE65904 datasets were accordingly divided into high- and low-risk subgroups.
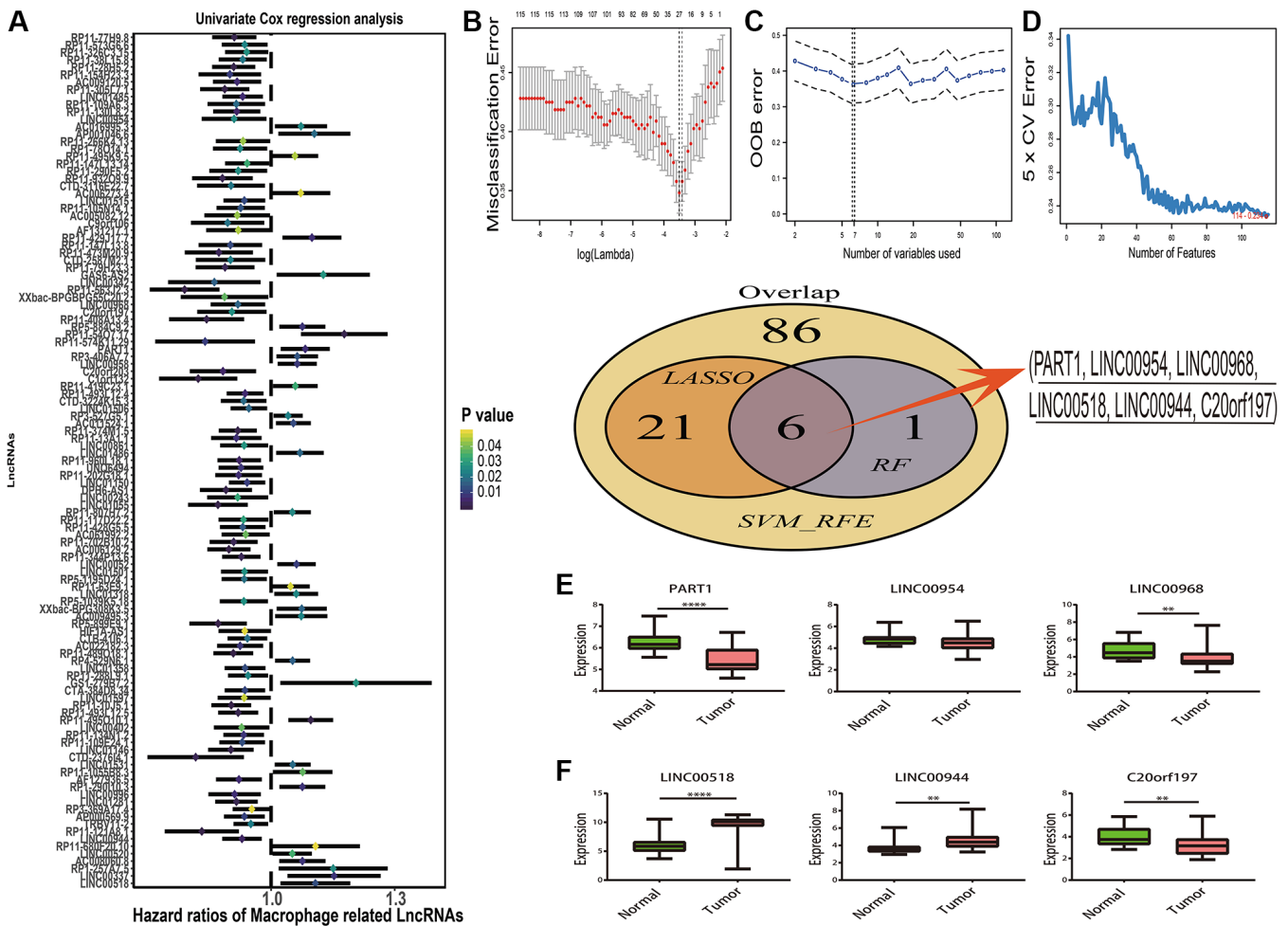


**Figure 2. Prognostic macrophage associated differentially expressed lncRNAs (DEMlncRNAs) feature selection.** (**A**) Forest plots of the prognostic DEMlncRNAs in training dataset. (**B**) Misclassification error distribution with the corresponding λ-logarithm value and the left variants of model in The Least Absolute Shrinkage and Selection Operator (LASSO) algorithm. (**C**) Random forests variable selection (RF-VS) algorithm. The lowest point of the curve indicates the lowest out of bag (OOB) error, and the corresponding DEMlncRNAs at this point are the best signature selected by RF-VS. (**D**) Support Vector Machine-Recursive Feature Elimination (SVM-RFE) algorithms. The point highlighted indicates the lowest error rate, and the corresponding DEMlncRNAs at this point are the best signature selected by SVM-RFE. (**E**) The Venn plot of overlapping DEMlncRNAs selected by LASSO, RF-VS and SVM-RFE algorithms. (**F**) Boxplots of lncRNA expression distribution in GSE15605 dataset.

KM curves indicated that significantly distinct survival outcome was also observed at high- and low-risk group in validation dataset with log-rank $p < 0.001$ (Figure 4C) and GSE65904 dataset with log-rank $p = 0.026$ (Figure 4E). The 3-, 5-year of AUCs were 0.778, 0.764 in validation dataset (Figure 4D) and 0.636, 0.622 (Figure 4F) in GSE65904 dataset respectively.

**Independence of the risk score from traditional clinical variables**

In uni- and multi-variate Cox regression analysis, the risk score and conventional clinical parameters were utilized to establish if the DEMlncRNAs signature is an independent predictive predictor of OS in various datasets. The train and validation datasets demonstrated that the DEMlncRNAs signature risk score and tumor stage were substantially linked with OS in both uni- and multi-variate Cox analysis (Figure 5A, 5B). In same analyses of an external GSE65904 dataset, the risk score was remained strongly linked with OS (Figure 5C). These findings suggest that the risk score of the

DEMlncRNAs signature is a significant predictive factor that is independent of other conventional clinical factors.

**Pathway enrichment analysis**

Overall, 53 lncRNA-paired protein-coding genes were predicted on the ENCORI website and utilized in BP term and KEGG pathway enrichment analyses. The KEGG enrichment results showed that these paired protein-coding genes were considerably enriched in biological processes linked to RNA transport, the mRNA surveillance pathway, and ribosome synthesis in eukaryotes, transcriptional misregulation in cancer, Herpes simplex infection and Spliceosome (Figure 4G). The BP findings indicated that these paired protein-coding genes were considerably enriched in pathways such as viral gene expression, gene expression regulation, epigenetics, positive control of translation, and 3′-UTR-mediated mRNA destabilization, regulation of telomere maintenance (Figure 4H). Furthermore, Based on ImmLnc database, these DEMlncRNAs
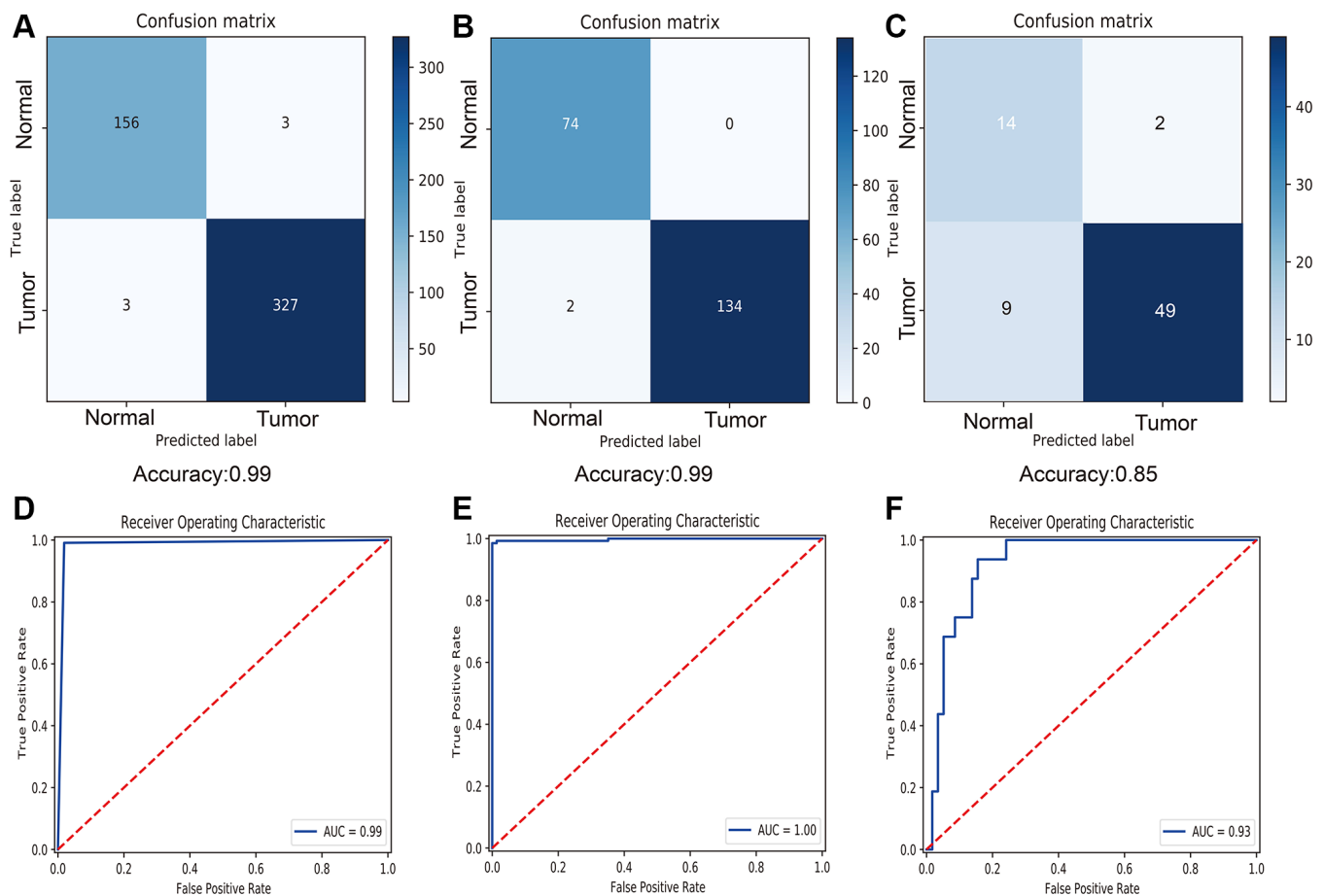


**Figure 3. Diagnostic performance of six selected macrophage associated lncRNAs.** (**A**) Confusion matrix of diagnostic prediction for melanoma in train dataset. (**B**) Confusion matrix of diagnostic prediction for melanoma in test dataset. (**C**) Confusion matrix of diagnostic prediction for melanoma in GSE15605 dataset. (**D**) Receiver operating characteristic (ROC) curve of diagnostic model in train dataset. (**E**) ROC curve of diagnostic model in test dataset. (**F**) ROC curve of diagnostic model in GSE15605 dataset.

significantly associated with immune pathways, including TNF family members, natural killer cell cytotoxicity, interleukins receptor and cytokine Receptors (Figure 4I). The detail results of pathway enrichment analysis were listed in Supplementary Table 4.

## Associations between risk score and conventional variables as well as the immunological microenvironment

Box plots demonstrated that clark level, tumor size, radiation, vital status, and metastatic status were associated with risk score (Figure 6A). To investigate the relationships between risk score and immunological microenvironment, the CIBERSORT algorithm was employed to calculate the relative proportions of 22 immune cells. Only 133 melanoma samples and 11

immune cells were selected out for further research based on the selection criteria. In overall, the 11 immune cell subsets in melanoma included memory B cells, naïve B cells, resting Mast cells, and M0, M1, M2 macrophages, resting NK cells, CD 8 T cells, follicular helper T cells, regulatory Tregs T cells and CD4 memory T cells have been activated, whose sum of mean proportions was more than 75% in all melanoma samples (Figure 6B). The differences in immune cell infiltrations between high- and low-risk groups were explored, and the findings revealed that Macrophages M0, M1, CD8, follicular helper, regulatory Tregs and CD4 memory activated T cells were differently infiltrated (Figure 6C). Afterwards, a total of 25 promising immune associated signatures were scored and classified into six categories which contained immune related biomarker, immune microenvironment,
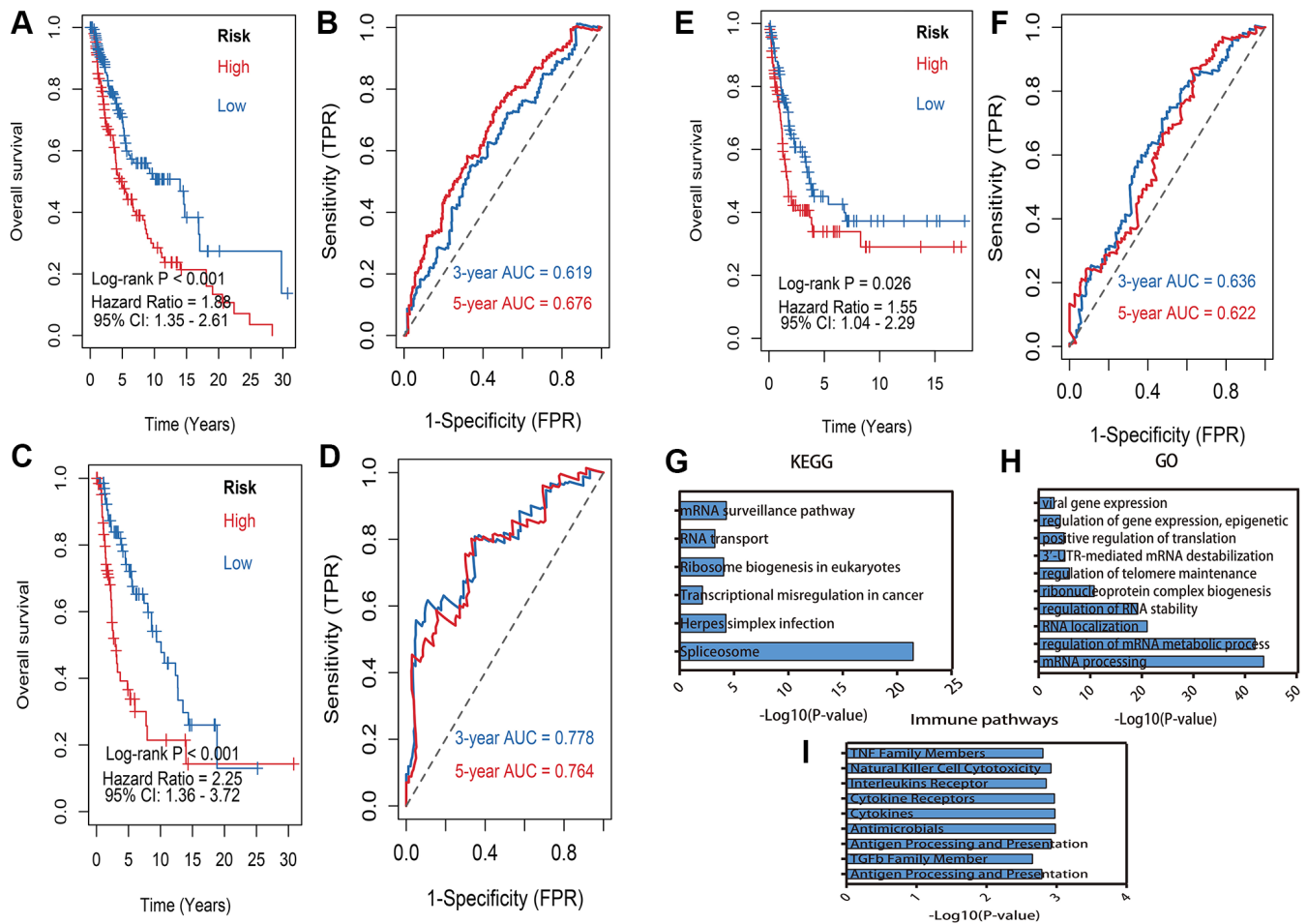


**Figure 4. Kaplan–Meier survival analysis and pathway enrichment.** (**A**) Kaplan–Meier survival analysis of risk model in train dataset. (**B**) 3, 5 years of the receiver operating characteristic (ROC) curves in train dataset. (**C**) Kaplan–Meier survival analysis of risk model in validation dataset. (**D**) 3, 5 years of the receiver operating characteristic (ROC) curves in validation dataset. (**E**) Kaplan–Meier survival analysis of risk model in GSE65904 dataset. (**F**) 3, 5 years of the receiver operating characteristic (ROC) curves in GSE65904 dataset. (**G**) Enriched Kyoto Encyclopedia of Genes and Genomes (KEGG) pathways of lncRNA-related mRNAs: X-axis means the -log10(*p*-value) of enrichment, Y-axis means pathway terms. (**H**) The biology process (BP) pathway enrichment of lncRNA-related: X-axis means the -log10(*p*-value) of enrichment, Y-axis means pathway terms. (**I**) The immune related pathway enrichment: X-axis means the -log10(*p*-value) of enrichment, Y-axis means pathway terms.

immune suppression, immune exclusion, immune exhaustion, T-cell or B-cell receptor (TCR_BCR). The heatmaps delineated a different immune expressed pattern between high and low risk phenotype regardless by using PCA (Figure 7A), ssGSEA (Figure 7B) or Z-score (Figure 7C) methods.
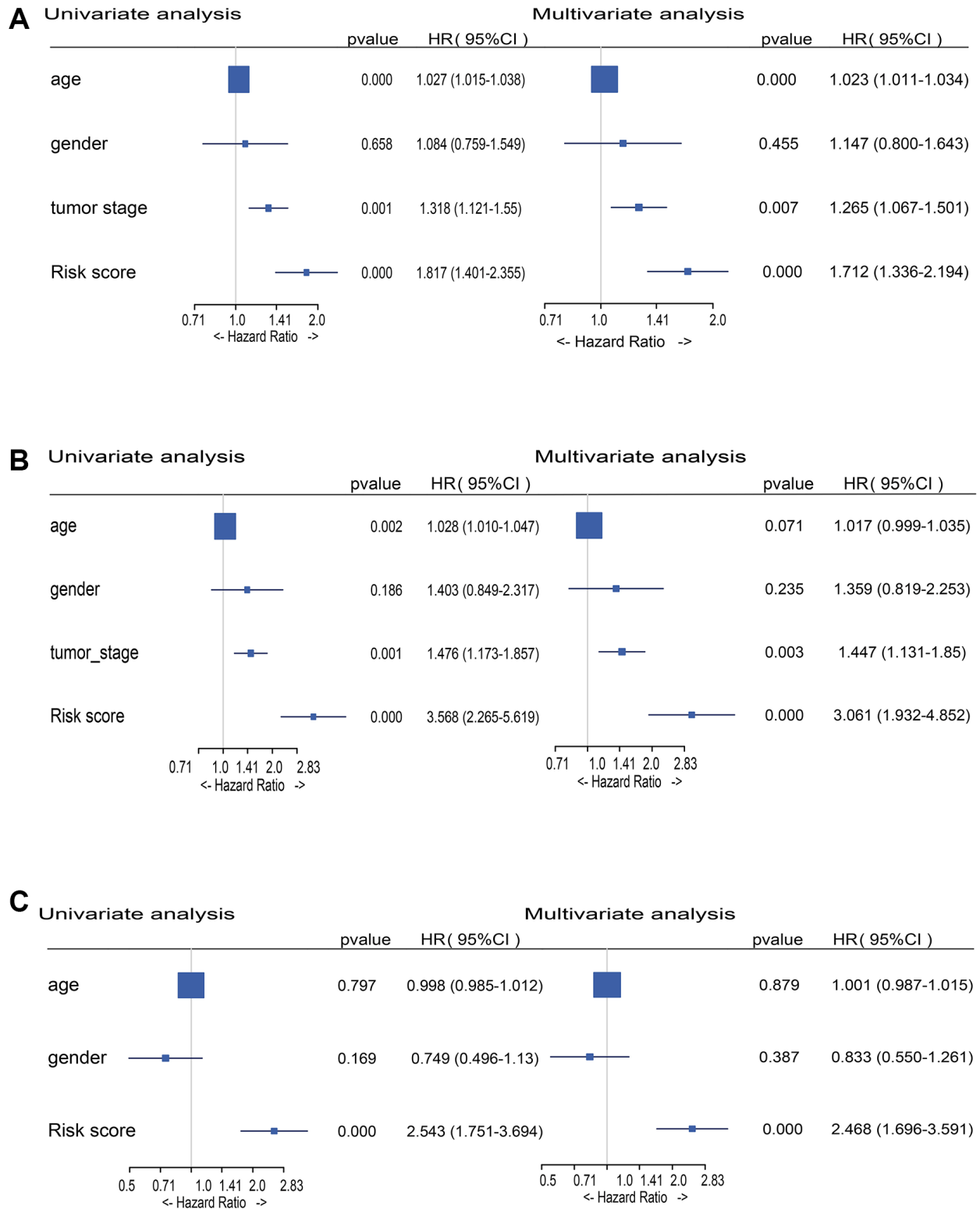


**Figure 5. Forest plot of risk score and traditional clinical variables in uni- and multivariate Cox regression.** (**A**) Hazard Ratios (HRs) of uni- and multivariate Cox analysis in TCGA-SKCM train dataset. (**B**) HRs of uni- and multivariate Cox analysis in TCGA-SKCM validation dataset. (**C**) HRs of uni- and multivariate Cox analysis in GSE65904 dataset.

## Comparison of risk score and previously identified prognostic indicators

In order to correlate our assessment of risk score with other established prognostic markers, several well established prognostic markers such as transcriptomic classification, mutation subtype and BRAF mutant for cutaneous melanoma were obtained from the previous TCGA study [25]. The TCGA research proven that patient in "immune" subtype of transcriptomic
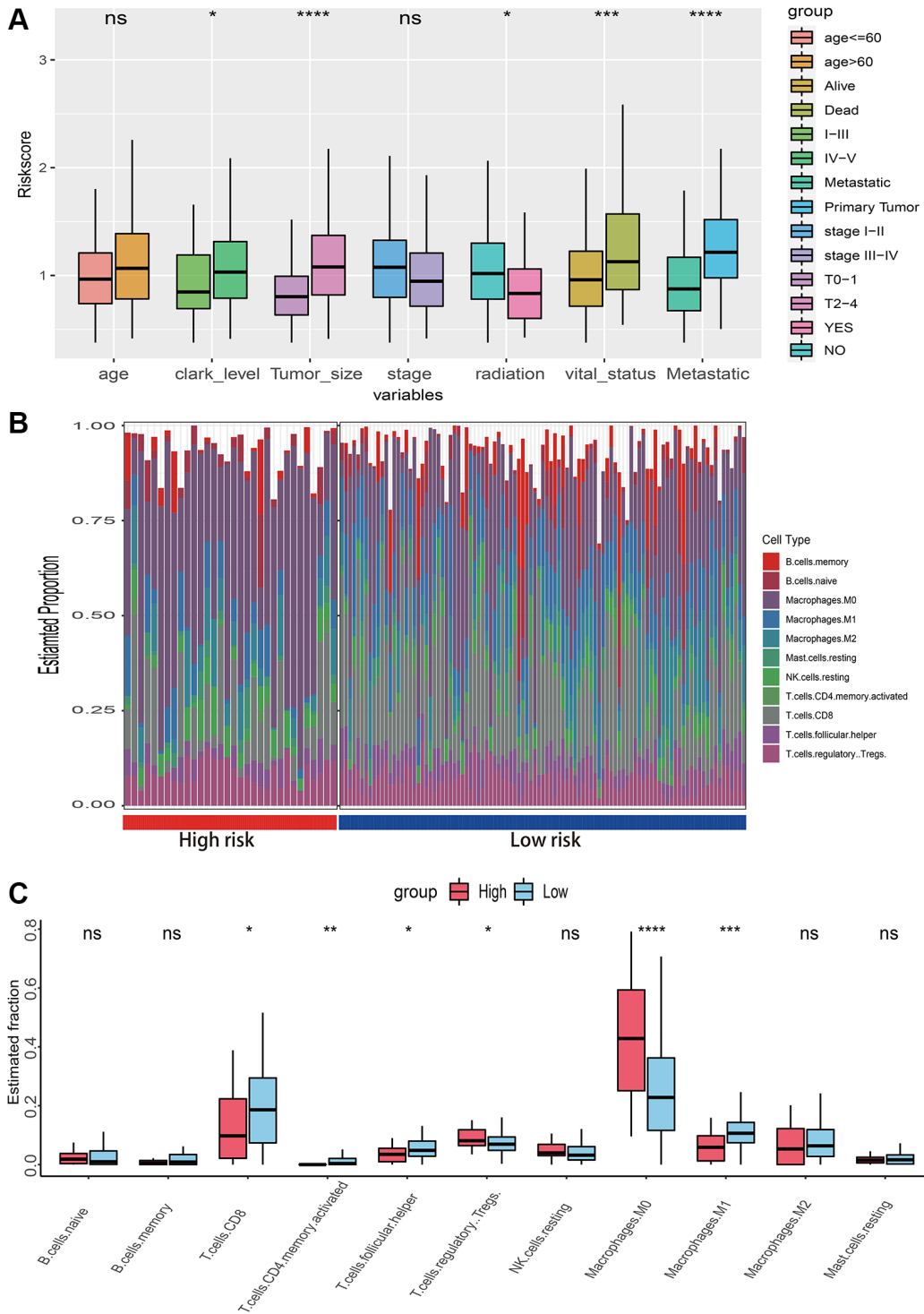


**Figure 6. Relationships between risk score with clinical characteristics and immune microenvironment.** (**A**) The risk score distribution of clinical variables which including age, clark level, tumor size, stage, radiation, vital status and metastatic status. (**B**) The landscape of immune infiltration between high and low risk groups in TCGA-SKCM dataset. (**C**) The difference of 11 immune infiltration between high and low risk groups; $^*p < 0.05$; $^{**}p < 0.01$; $^{***}p < 0.001$; $^{****}p < 0.0001$.

classifications (Figure 8A), "BRAF Hotspot Mutants" of mutation subtypes (Figure 8C) and BRAF mutant group (Figure 8E) have a good prognosis, respectively. The risk distribution of these well established prognostic markers suggested that "MITF low" subtype (Figure 8B), "Triple WT" mutant subtype (Figure 8D) and BRAF wildtype group (Figure 8F) have a higher risk score than "immune" subtype, "BRAF Hotspot Mutants" subtypes and BRAF mutant group, respectively. Most importantly, compared with the 5 years AUC values of these established prognostic markers (transcriptomic classification, mutation subtype, tumor stage and BRAF mutant), our signature can achieve higher accuracy value (Figure 8G).

**Potential indicator for melanoma immunotherapy**

The relationship between risk score and immune checkpoint gene expression (PD-1 and CTLA-4) was investigated further to assess the potential responsiveness to immunotherapy. According to the

Spearman tests, the estimated risk score was substantially negatively linked with PD-1 expression (r = −0.4883; $p < 0.0001$) (Figure 9A) and CTLA-4 expression (r = −0.2574; $p < 0.0001$) (Figure 9C). The stratified analysis indicated that PD-1 (Figure 9B) and CTLA-4 (Figure 9D) in the low risk subgroup had significant higher expression levels than those in high risk subgroup. The cross-talk influences of the risk score and immune checkpoint genes on patient survival were further analyzed. Based on the combination of risk score and immune checkpoint genes, these patients were classified into four categories, and KM curve analyses were performed to assess the various survival outcomes among the four subgroups. When compared to the data, the risk score was able to discriminate patients' outcomes with opposing levels of immune checkpoint genes (Figure 9E, 9F). Patients with high risk scores and low levels of immune checkpoint genes fared the poorest. Patients with low risk scores and high levels of immune checkpoint genes, on the other hand, are more likely to survive longer among the four groups.
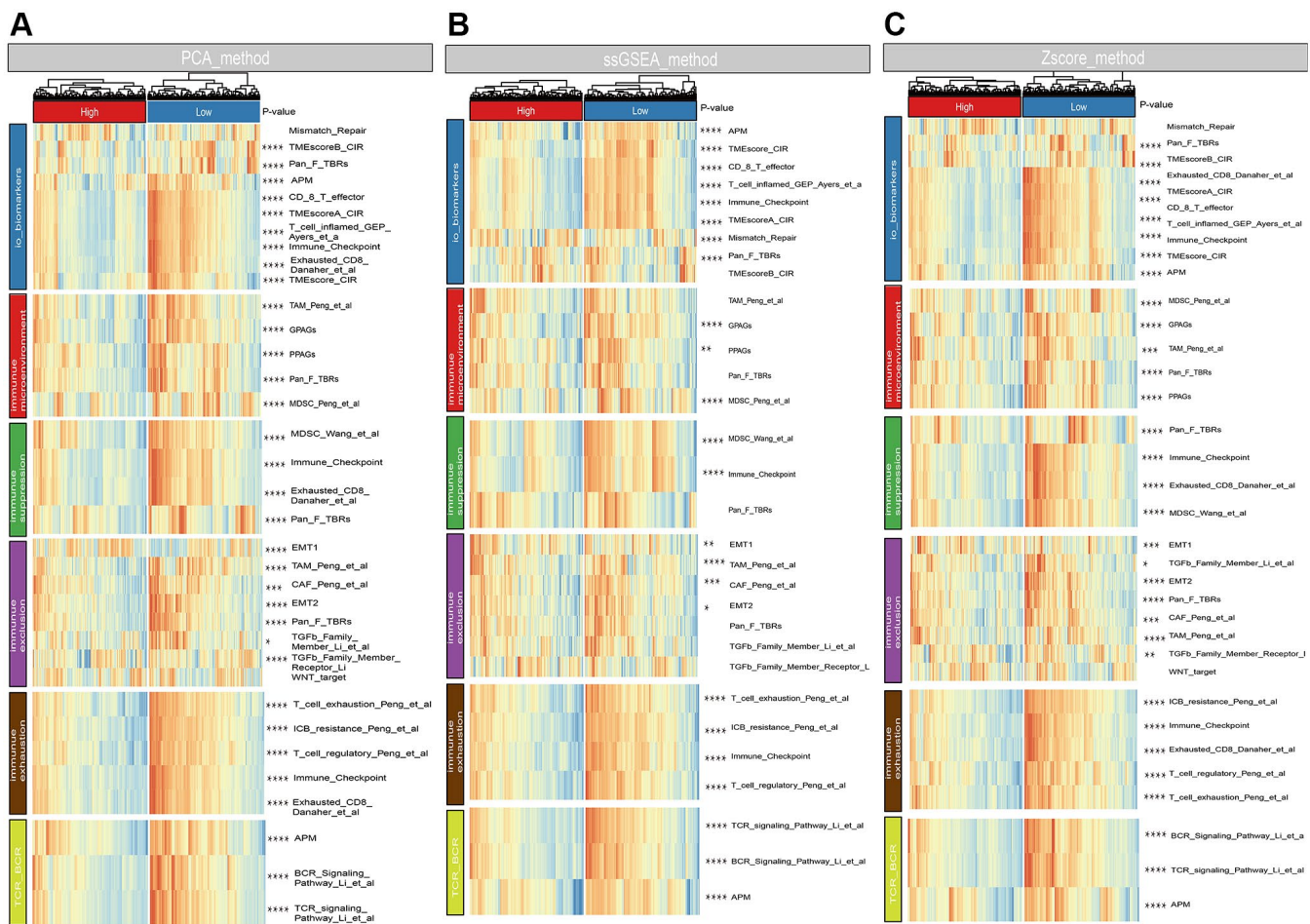


**Figure 7. Associations between risk score and immune signatures.** (**A**) Heatmap for immune related signatures between high and low risk subgroup based on Principal Component Analysis (PCA) method. (**B**) Heatmap for immune related signatures between high and low risk subgroup based on Single-sample Enrichment Analysis (ssGSEA) methods. (**C**) Heatmap for immune related signatures between high and low risk subgroup based on Z-score method.

Because of the strong association between the risk score and immune checkpoint genes, we postulated that the risk score may be used to predict response to melanoma immunotherapy. As a consequence, we conducted the TIDE method and subclass mapping to predict melanoma who responded to immune-checkpoint inhibitors (CTLA-4 and PD-1) [22]. Strikingly, the low risk group reacts better to anti-PD-1 therapy (Bonferroni adjusted $P = 0.007$) (Figure 10A). Patients in the high-risk category, on the other hand, do not respond to anti-CTLA-4 therapy (Bonferroni corrected $P = 0.039$) (Figure 10A). To validate our hypothesis, participants in the Riaz et al. and Hugo et al. melanoma studies who received anti-PD-1 treatment were divided into low and high risk score groups [20, 21]. Notably, individuals in high risk group have a poor prognosis regardless in Hugo et al. cohort (Figure 10B) or Riaz et al. cohort (Figure 10C). Furthermore, in the Hugo et al cohort (Figure 10D) and Riaz et al. cohort (Figure 10E), the non-respond group had a higher risk score than the response group for anti-PD-1 immunotherapy.

**Gene set enrichment analysis (GSEA)**

GSEA was used to examine the distinct activation of cancer hallmarks between low and high risk groups for investigating the potential biological and molecular mechanism of the lncRNA signature. We found that 10 positive linked pathways were enriched in the low risk group, which included interferon alpha and gamma response, allograft rejection, inflammatory response, epithelial mesenchymal transition, TNFA signaling through NFKB (Figure 10F). Oxidative phosphorylation, MYC targets, estrogen response late, estrogen response early, and KRAS signaling were all actively related with the high risk group (Figure 10F).

## DISCUSSION

The risk and morbidity of melanoma patients increase rapidly. Once it has spread, it is much harder to improve the chance of melanoma-specific survival at all [27]. Cancer immunotherapy is currently recognized as a
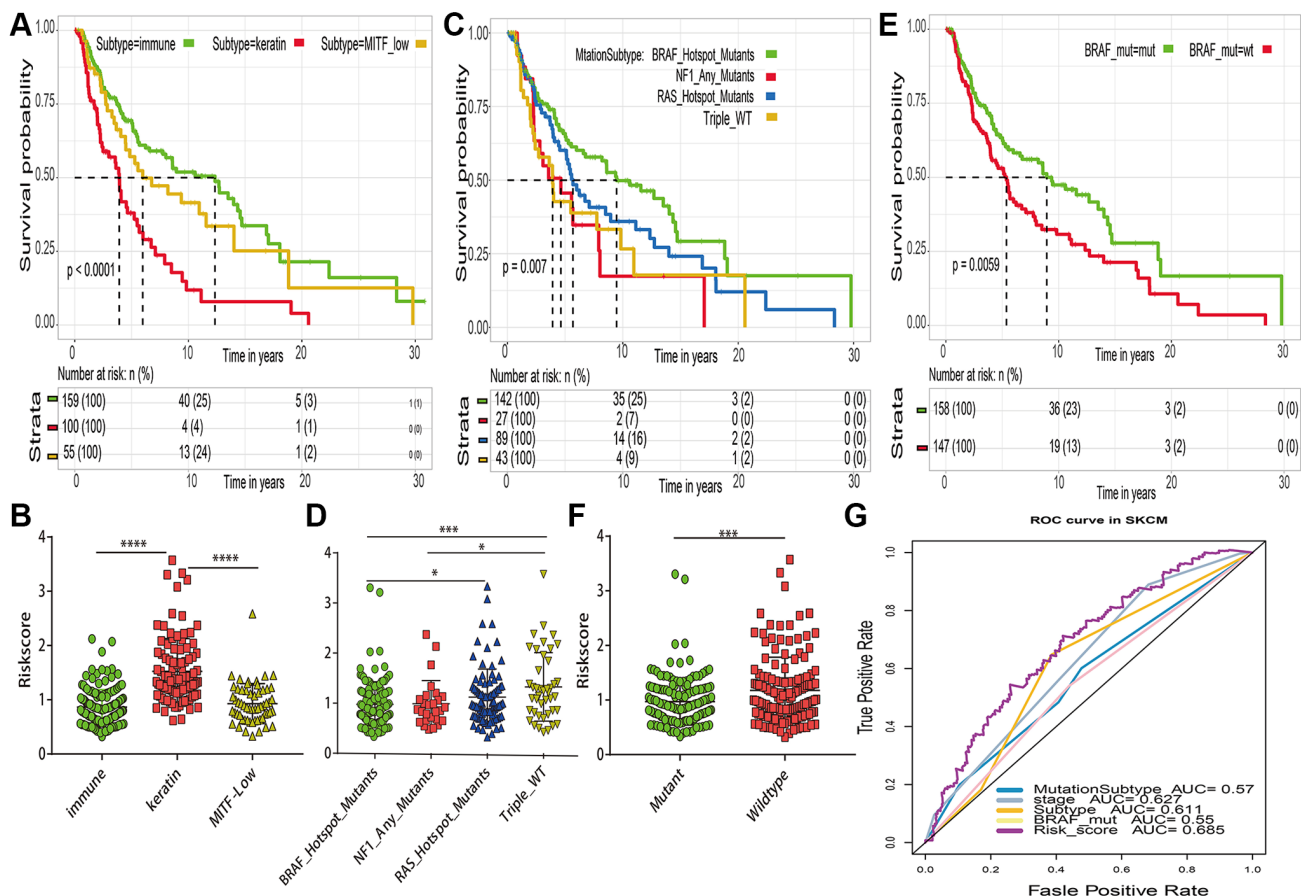


**Figure 8. Comparations between risk score and previously established prognostic markers in TCGA-SKCM.** (**A**) Kaplan–Meier survival curve of transcriptomic subtypes. (**B**) The risk score distribution of transcriptomic subtypes (named "immune", "keratin" and "MITF-low). (**C**) Kaplan–Meier survival curve of mutation subtypes (named BRAF subtype, RAS subtype, NF1 subtype and Triple Wild-Type subtype). (**D**) The risk score distribution of mutation subtypes. (**E**) Kaplan–Meier curve of BRAF mutant. (**F**) The risk score distribution of BRAF mutant and wildtype. (**G**) The 5 years area under the curve (AUC) of risk score and prognostic markers associated with overall survival. $^{*}p < 0.05$; $^{**}p < 0.01$; $^{***}p < 0.001$; $^{****}p < 0.0001$.

potential treatment approach that is commonly employed in melanoma patients [28, 29]. Nevertheless, not all melanomas are responding to immunotherapy and even in the subtype of those tumor. These differential outcomes not only caused by the heterogeneity of tumor, but also resulted in tumor microenvironment composition [30, 31]. Immune cells of the tumor microenvironment are critically involved in response of immunotherapy. As a key component of infiltrating immune cells, macrophage has been
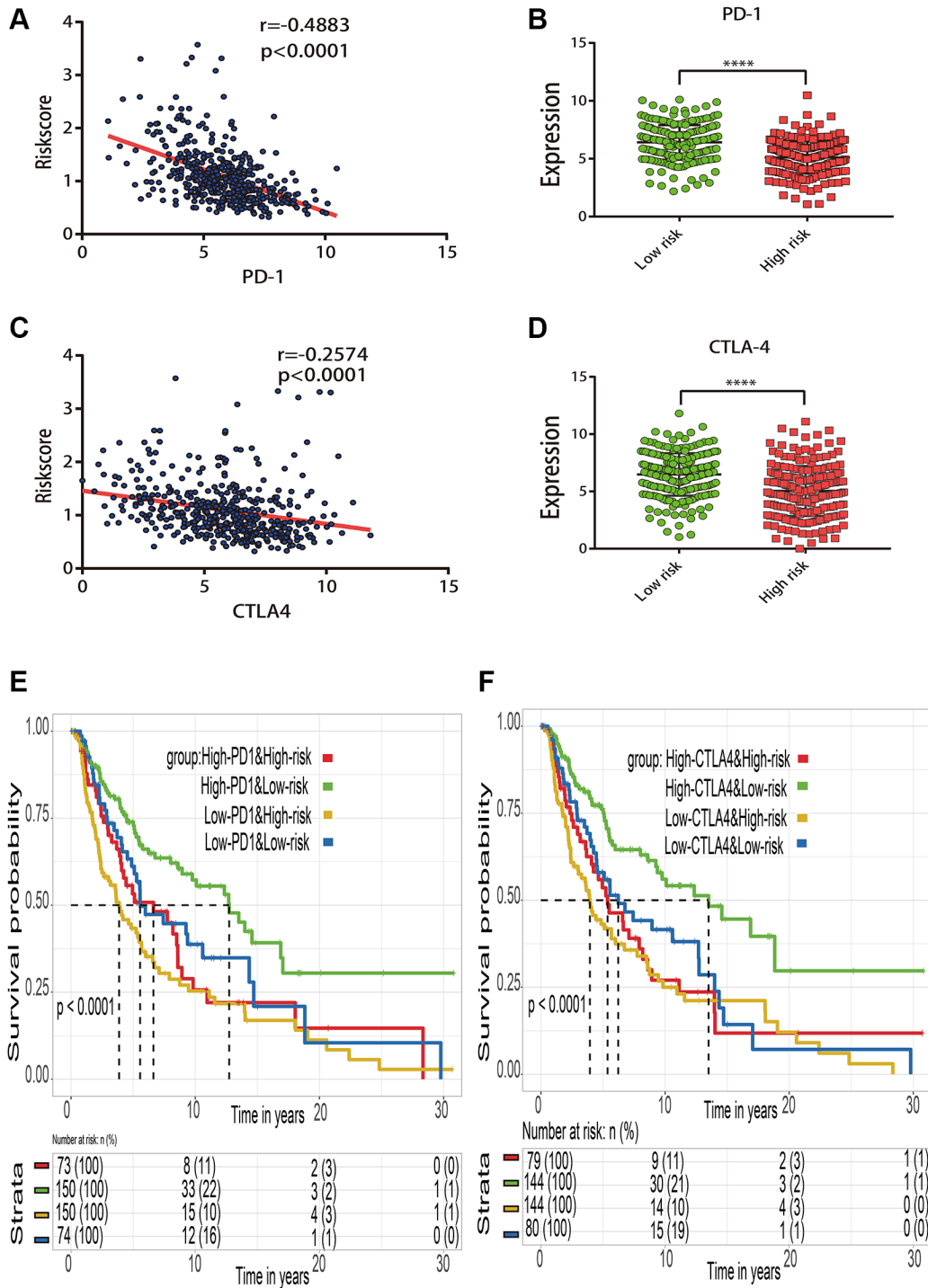


**Figure 9. Effect of the risk score and immune checkpoint gene expression on patient survival.** (**A**) Correlation between the risk score and PD-1 gene expression. (**B**) Expression distribution of PD-1 gene in the high- and low-risk groups stratified by risk score. (**C**) Correlation between the risk score and CTLA4 gene expression. (**D**) Expression distribution of CTLA4 gene in the high- and low-risk groups stratified by risk score. (**E**) Kaplan–Meier survival curve of four groups stratified by the risk score and PD-1 expression. (**F**) Kaplan–Meier survival curve of four groups stratified by the risk score and CTLA4 expression.

identified that it's activities could dysregulate immune activity, enhance tumor metastasis, upregulate immune response evasion and effect other immune cells [32–34].

Besides, recent studies revealed that lncRNAs are widely regulated cancer immunity. Several bigdata analyses suggested that the cell-type specificity of
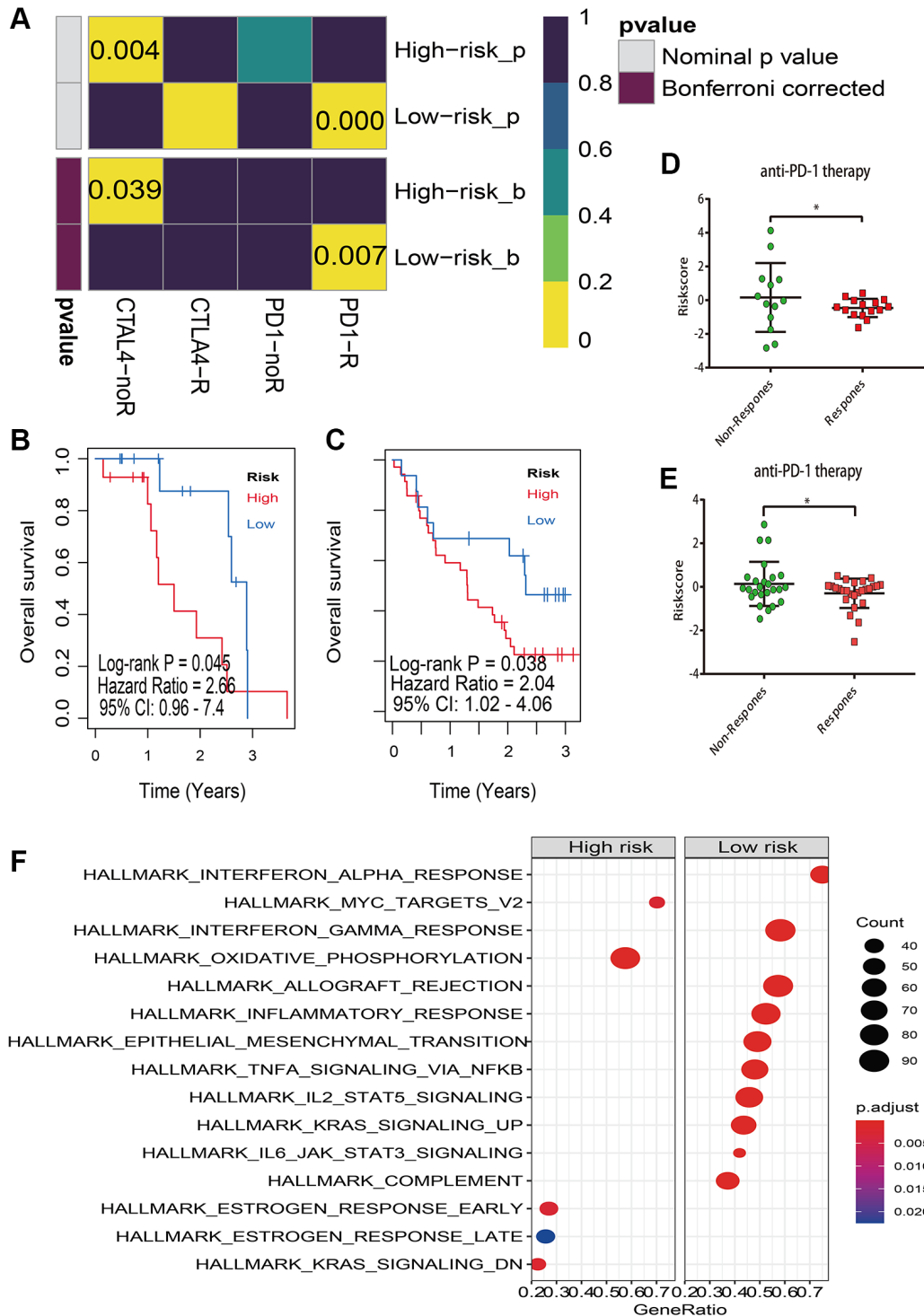


**Figure 10. Immunotherapy response prediction.** (**A**) Submap analysis manifested that low risk group could be more sensitive to the PD-1 inhibitor (Bonferroni-corrected *P* = 0.07), and high risk group are insensitive to anti-CTLA-4 therapy (Bonferroni corrected *P* = 0.039); (**B**) Kaplan–Meier survival analysis of risk model in Hugo et al melanoma study (accession number: GSE78220); (**C**) Kaplan–Meier survival analysis of risk model in Riaz et al melanoma study (accession number: GSE91061); (**D**) The risk score distribution of anti-PD-1 therapy between response and non-response in GSE78220; (**E**) The risk score distribution of anti-PD-1 therapy between response and non-response in GSE91061; (**F**) Gene set enrichment analysis (GSEA) of high vs low risk scores groups in cancer hallmark pathways.

lncRNA can work as a potential marker for the subpopulation of immune cells [35, 36]. Hence, it is necessary to elucidate the accurate molecular regulation of macrophage polarization to increase the efficacy of tumor-infiltrated macrophage targeted methods and immunotherapy response in melanoma.

Therefore, in this study, multiple machine learning algorithms were applied to select potential lncRNAs from the list of macrophage associated lncRNAs and established a diagnostic and prognostic signature, which also was verified in validation and external sets. The diagnostic and prognostic signature contained six lncRNAs, including PART1, LINC00968, LINC00954, LINC00944, LINC00518 and C20orf197. Among these macrophage-related lncRNAs, several have been demonstrated to link with cancer or immunological response. For example, the PART1 lncRNA can modulate Toll-like receptor pathways to effect the immune response and cell apoptosis [37]. Recent experimental results manifested that the inhibition of LINC00968 can significantly decrease the proliferation of tumor cell and could be regard as an oncogene in various cancers [38, 39]. Luan at el also suggested that LICN00518 was highly expressed in melanoma tissues and could be an independent risk indicator for melanoma patients [40]. The enrichment of these lncRNAs in immune response-related pathways, such as TNF family members, natural killer cell cytotoxicity, and interleukin receptors, suggests their potential involvement in modulating the interactions between tumor-infiltrating macrophages and the immune microenvironment within melanoma. These lncRNAs may exert regulatory effects on the expression of key immune-related genes, cytokines, and receptors, thereby influencing the polarization and function of macrophages and other immune cells in the tumor microenvironment. Furthermore, the association of these lncRNAs with cytokine receptors and RNA synthesis-related signaling pathways, including mRNA surveillance, RNA transport, and transcriptional misregulation in cancer, indicates their potential roles in coordinating the expression and processing of immune-related genes and signaling molecules. It is conceivable that these lncRNAs may participate in the post-transcriptional and post-translational regulation of immune response genes, affecting the secretion and activity of cytokines and chemokines involved in melanoma-immune cell crosstalk.

To estimate the accurate ability of survival prediction, we also built risk score model and classified melanomas into high- or low-risk group. The KM survival curves showed that low-risk patients have a good prognosis. Compared with the traditional clinical factors, the multivariate Cox results in different cohorts

suggested that the risk score might be independently considered as a prognostic biomarker. Moreover, the distribution of risk score in clinical features manifiested that the high risk score was closely associated with high clark level, large tumor size, no radiation and metastasis. Besides, the high-risk patients had higher macrophage infiltration and lower T cell infiltration than low risk group. T cells act as cytotoxic lymphocytes, and once fully cytotoxic, they are critical in suppressing the proliferation of cancer cells and growth through the immune system [41]. However, the increasingly infiltrated myeloid cells such as macrophages, and dendritic cells would enhance cancer cells expansion, immune surveillance evasion, and eventually lead to metastasis [42, 43]. Most importantly, we astonishingly observed that our macrophage associated lncRNAs signature defined low-risk melanoma patients who were belong to immune inflamed subtype and have strong immuno-stimulating functions of suppression, exclusion, and exhaustion. Therefore, it goes without saying that our lncRNA related signature closely associated with immune activation and prognosis of melanoma. Furthermore, the risk score distributions of transcriptomic classification, mutation subtype and BRAF mutant showed that "keratin", "Triple WT" subtypes and wildtype of BRAF were significantly higher than "immune", "BRAF Hotspot Mutants" and mutant of BRAF in melanoma, which was in line with prior findings. Notably, when compared to the AUC values of well-established prognostic biomarkers such as stage, transcriptome categorization, mutation subtype, and BRAF mutant over a 5-year period, our lncRNA associated biomarker achieves a higher accuracy value.

At present, checkpoint blockade immunotherapies were emerging as a promising strategy and reveal a great benefit in cancer therapy. Especially, PD-1 and CTLA-4 blocking antibodies are widely used in clinical melanoma treatment [44–46]. However, only a portion of patients are responding to immune checkpoint inhibitor therapy. Therefore, it's essentially to identify the predicted roles for immune checkpoint immunotherapy responses. When checking the associations between DEMlncRNAs signature and PD-1/CTLA-4, the risk score of DEMlncRNAs signature showed a significantly correlated with the PD-1 and CTLA-4 expression. In addition, the combination of survival analyses between DEMlncRNAs signature and immune checkpoint genes indicated an interacted influence on the prognosis of patients. Our results are consistent with recent researches that the PD-1 expression of tumor-infiltrating macrophage negatively correlates with the function of macrophage for against tumor cells [47]. The synthesis of PD-1 blockade with

macrophage associated treatment will enhance immunotherapy effect in cancer therapy [48]. Hence, our DEMlncRNAs related signature might be used to predict melanoma treatment response. However, it is uncertain whether types of melanomas are amenable to immune checkpoint inhibitor treatment. Thus, the subgroup with varied risk scores was investigated in many published datasets that reacted to immune-checkpoint inhibitors. We were surprised to discover that the low-risk group is likely to respond to anti-PD-1 treatment, whereas the high-risk group is insensitive to anti-CTLA-4 treatment, which could supply effective solutions to aid in the final clinical decision and help patients with advanced melanoma achieve the highest remission rate.

Moreover, we discovered that immunological pathways such interferon alpha and gamma response, inflammatory response, allograft rejection, and TNFA signaling through NFKB were favorably active in the low-risk phenotype using GSEA. Interferon alpha and gamma signaling is well recognized as an important effector in anti-cancer immune response [49]. NFKB is essential for the control of immunological responses and inflammation [50]. As a result, it's clear to see why low-risk melanoma patients have a greater survival rate and respond better to immunotherapy.

## CONCLUSION

In summary, our study comprehensively identified several lncRNAs related signatures by integrative analysis of immune related lncRNA, tumor-infiltrating macrophage and clinical features. And we also proven the efficiency of signature in predicting prognosis and immunotherapy response of melanoma, which may give a more simple and reliable prediction for melanoma patients and provide a framework to evaluate potential population for immunotherapy. Furthermore, to the best of our knowledge, this is the first study to investigate the tumor-infiltrated macrophage associated lncRNA signature, emphasizing the role of lncRNAs in macrophage infiltration and paving the way for future individual melanoma immunotherapy.

### Abbreviations

lncRNA: long noncoding RNA; DEMlncRNAs: Differential expressed macrophage associated lncRNAs; TCGA: The Cancer Genome Atlas database; GEO: Gene Expression Omniniub; LASSO: Least Absolute Shrinkage and Selection Operator; SVM-RFE: Support Vector Machine-Recursive Feature Elimination; RF-VS: Random Forests Variable selection; OS: overall survival; AUC: The area under the curve; ROC: Receiver operating characteristic curves.

## AUTHOR CONTRIBUTIONS

QW was in charge of writing; YHD was in charge of revising and editing; RW, KM and JT are responsible for the duty of editing; YPD was responsible for project administration.

## CONFLICTS OF INTEREST

## FUNDING

## REFERENCES

1. Lu X, Zhang Q, Wang Y, Zhang L, Zhao H, Chen C, Wang Y, Liu S, Lu T, Wang F, Yan F. Molecular classification and subtype-specific characterization of skin cutaneous melanoma by aggregating multiple genomic platform data. J Cancer Res Clin Oncol. 2018; 144:1635–47.
https://doi.org/10.1007/s00432-018-2684-7
PMID:29948145

2. Kim SW, Kim YI, Mustafa B, Kim MJ, Jeong G, Ahn SM, Lim SB, Yu CS, Kim JC, Hong SM, Park IJ. Distribution pattern of tumor infiltrating lymphocytes and tumor microenvironment composition as prognostic indicators in anorectal malignant melanoma. Mod Pathol. 2021; 34:141–60.
https://doi.org/10.1038/s41379-020-0633-x
PMID:32709987

3. Wang P, Zhang X, Sun N, Zhao Z, He J. Comprehensive Analysis of the Tumor Microenvironment in Cutaneous Melanoma associated with Immune Infiltration. J Cancer. 2020; 11:3858–70.
https://doi.org/10.7150/jca.44413
PMID:32328190

4. Mao S, Li Y, Lu Z, Che Y, Huang J, Lei Y, Wang Y, Wang X, Liu C, Zheng S, Li N, Li J, Sun N, He J. Systematic profiling of immune signatures identifies prognostic predictors in lung adenocarcinoma. Cell Oncol (Dordr). 2020; 43:681–94.
https://doi.org/10.1007/s13402-020-00515-7
PMID:32462608

5. Falleni M, Savi F, Tosi D, Agape E, Cerri A, Moneghini L, Bulfamante GP. M1 and M2 macrophages'

clinicopathological significance in cutaneous melanoma. Melanoma Res. 2017; 27:200–10.
https://doi.org/10.1097/CMR.0000000000000352
PMID:28272106

6. Italiani P, Boraschi D. From Monocytes to M1/M2 Macrophages: Phenotypical vs. Functional Differentiation. Front Immunol. 2014; 5:514.
https://doi.org/10.3389/fimmu.2014.00514
PMID:25368618

7. Wang D, Wang X, Si M, Yang J, Sun S, Wu H, Cui S, Qu X, Yu X. Exosome-encapsulated miRNAs contribute to CXCL12/CXCR4-induced liver metastasis of colorectal cancer by enhancing M2 polarization of macrophages. Cancer Lett. 2020; 474:36–52.
https://doi.org/10.1016/j.canlet.2020.01.005
PMID:31931030

8. Fu LQ, Du WL, Cai MH, Yao JY, Zhao YY, Mou XZ. The roles of tumor-associated macrophages in tumor angiogenesis and metastasis. Cell Immunol. 2020; 353:104119.
https://doi.org/10.1016/j.cellimm.2020.104119
PMID:32446032

9. Scali E, Mignogna C, Di Vito A, Presta I, Camastra C, Donato G, Bottoni U. Inflammation and macrophage polarization in cutaneous melanoma: Histopathological and immunohistochemical study. Int J Immunopathol Pharmacol. 2016; 29:715–9.
https://doi.org/10.1177/0394632016650895
PMID:27387897

10. Wang H, Zhang L, Yang L, Liu C, Zhang Q, Zhang L. Targeting macrophage anti-tumor activity to suppress melanoma progression. Oncotarget. 2017; 8:18486–96.
https://doi.org/10.18632/oncotarget.14474
PMID:28060744

11. Lu L, Yu X, Zhang L, Ding X, Pan H, Wen X, Xu S, Xing Y, Fan J, Ge S, Zhang H, Jia R, Fan X. The Long Non-Coding RNA RHPN1-AS1 Promotes Uveal Melanoma Progression. Int J Mol Sci. 2017; 18:226.
https://doi.org/10.3390/ijms18010226
PMID:28124977

12. Hauptman N, Glavač D. Long non-coding RNA in cancer. Int J Mol Sci. 2013; 14:4655–69.
https://doi.org/10.3390/ijms14034655
PMID:23443164

13. Djebali S, Davis CA, Merkel A, Dobin A, Lassmann T, Mortazavi A, Tanzer A, Lagarde J, Lin W, Schlesinger F, Xue C, Marinov GK, Khatun J, et al. Landscape of transcription in human cells. Nature. 2012; 489:101–8.
https://doi.org/10.1038/nature11233
PMID:22955620

14. Sheng L, Wei R. Long Non-Coding RNA-CASC15 Promotes Cell Proliferation, Migration, and Invasion by Activating Wnt/β-Catenin Signaling Pathway in Melanoma. Pathobiology. 2020; 87:20–9.
https://doi.org/10.1159/000502803
PMID:31838468

15. Li Q, Liu Q. Noncoding RNAs in Cancer Immunology. Adv Exp Med Biol. 2016; 927:243–64.
https://doi.org/10.1007/978-981-10-1498-7_9
PMID:27376738

16. Elling R, Robinson EK, Shapleigh B, Liapis SC, Covarrubias S, Katzman S, Groff AF, Jiang Z, Agarwal S, Motwani M, Chan J, Sharma S, Hennessy EJ, et al. Genetic Models Reveal cis and trans Immune-Regulatory Activities for lincRNA-Cox2. Cell Rep. 2018; 25:1511–24.e6.
https://doi.org/10.1016/j.celrep.2018.10.027
PMID:30404006

17. Liu B, Sun L, Liu Q, Gong C, Yao Y, Lv X, Lin L, Yao H, Su F, Li D, Zeng M, Song E. A cytoplasmic NF-κB interacting long noncoding RNA blocks IκB phosphorylation and suppresses breast cancer metastasis. Cancer Cell. 2015; 27:370–81.
https://doi.org/10.1016/j.ccell.2015.02.004
PMID:25759022

18. Krawczyk M, Emerson BM. p50-associated COX-2 extragenic RNA (PACER) activates COX-2 gene expression by occluding repressive NF-κB complexes. Elife. 2014; 3:e01776.
https://doi.org/10.7554/eLife.01776
PMID:24843008

19. Li Y, Jiang T, Zhou W, Li J, Li X, Wang Q, Jin X, Yin J, Chen L, Zhang Y, Xu J, Li X. Pan-cancer characterization of immune-related lncRNAs identifies potential oncogenic biomarkers. Nat Commun. 2020; 11:1000.
https://doi.org/10.1038/s41467-020-14802-2
PMID:32081859

20. Hugo W, Zaretsky JM, Sun L, Song C, Moreno BH, Hu-Lieskovan S, Berent-Maoz B, Pang J, Chmielowski B, Cherry G, Seja E, Lomeli S, Kong X, et al. Genomic and Transcriptomic Features of Response to Anti-PD-1 Therapy in Metastatic Melanoma. Cell. 2016; 165:35–44.
https://doi.org/10.1016/j.cell.2016.02.065
PMID:26997480

21. Riaz N, Havel JJ, Makarov V, Desrichard A, Urba WJ, Sims JS, Hodi FS, Martín-Algarra S, Mandal R, Sharfman WH, Bhatia S, Hwu WJ, Gajewski TF, et al. Tumor and Microenvironment Evolution during Immunotherapy with Nivolumab. Cell. 2017; 171:934–49.e16.
https://doi.org/10.1016/j.cell.2017.09.028
PMID:29033130

22. Roh W, Chen PL, Reuben A, Spencer CN, Prieto PA, Miller JP, Gopalakrishnan V, Wang F, Cooper ZA, Reddy SM, Gumbs C, Little L, Chang Q, et al. Integrated molecular analysis of tumor biopsies on sequential CTLA-4 and PD-1 blockade reveals markers of response and resistance. Sci Transl Med. 2017; 9:eaah3560.
https://doi.org/10.1126/scitranslmed.aah3560
PMID:28251903

23. Ritchie ME, Phipson B, Wu D, Hu Y, Law CW, Shi W, Smyth GK. limma powers differential expression analyses for RNA-sequencing and microarray studies. Nucleic Acids Res. 2015; 43:e47.
https://doi.org/10.1093/nar/gkv007
PMID:25605792

24. Qiu J, Peng B, Tang Y, Qian Y, Guo P, Li M, Luo J, Chen B, Tang H, Lu C, Cai M, Ke Z, He W, et al. CpG Methylation Signature Predicts Recurrence in Early-Stage Hepatocellular Carcinoma: Results From a Multicenter Study. J Clin Oncol. 2017; 35:734–42.
https://doi.org/10.1200/JCO.2016.68.2153
PMID:28068175

25. Cancer Genome Atlas Network. Genomic Classification of Cutaneous Melanoma. Cell. 2015; 161:1681–96.
https://doi.org/10.1016/j.cell.2015.05.044
PMID:26091043

26. Wang T, Xiao M, Ge Y, Krepler C, Belser E, Lopez-Coral A, Xu X, Zhang G, Azuma R, Liu Q, Liu R, Li L, Amaravadi RK, et al. BRAF Inhibition Stimulates Melanoma-Associated Macrophages to Drive Tumor Growth. Clin Cancer Res. 2015; 21:1652–64.
https://doi.org/10.1158/1078-0432.CCR-14-1554
PMID:25617424

27. Chen XE, Chen P, Chen S, Lu J, Ma T, Shi G, Sheng L. Long non-coding RNA FENDRR inhibits migration and invasion of cutaneous malignant melanoma cells. Biosci Rep. 2020; 40:BSR20191194.
https://doi.org/10.1042/BSR20191194
PMID:32134466. Retraction in: Biosci Rep. 2023; 43.
https://doi.org/10.1042/BSR-2019-1194_RET
PMID:38131306

28. Babačić H, Lehtiö J, Pico de Coaña Y, Pernemalm M, Eriksson H. In-depth plasma proteomics reveals increase in circulating PD-1 during anti-PD-1 immunotherapy in patients with metastatic cutaneous melanoma. J Immunother Cancer. 2020; 8:e000204.
https://doi.org/10.1136/jitc-2019-000204
PMID:32457125

29. Leonardi GC, Candido S, Falzone L, Spandidos DA, Libra M. Cutaneous melanoma and the immunotherapy revolution (Review). Int J Oncol. 2020; 57:609–18.

https://doi.org/10.3892/ijo.2020.5088
PMID:32582963

30. Xu S, Wang Q, Kang Y, Liu J, Yin Y, Liu L, Wu H, Li S, Sui S, Shen M, Zheng W, Pang D. Long Noncoding RNAs Control the Modulation of Immune Checkpoint Molecules in Cancer. Cancer Immunol Res. 2020; 8:937–51.
https://doi.org/10.1158/2326-6066.CIR-19-0696
PMID:32321773

31. Zhang Y, Zhang L, Xu Y, Wu X, Zhou Y, Mo J. Immune-related long noncoding RNA signature for predicting survival and immune checkpoint blockade in hepatocellular carcinoma. J Cell Physiol. 2020; 235:9304–16.
https://doi.org/10.1002/jcp.29730
PMID:32330311

32. Cao J, Dong R, Jiang L, Gong Y, Yuan M, You J, Meng W, Chen Z, Zhang N, Weng Q, Zhu H, He Q, Ying M, Yang B. LncRNA-MM2P Identified as a Modulator of Macrophage M2 Polarization. Cancer Immunol Res. 2019; 7:292–305.
https://doi.org/10.1158/2326-6066.CIR-18-0145
PMID:30459152

33. Cassetta L, Kitamura T. Macrophage targeting: opening new possibilities for cancer immunotherapy. Immunology. 2018; 155:285–93.
https://doi.org/10.1111/imm.12976
PMID:29963704

34. Zhou YX, Zhao W, Mao LW, Wang YL, Xia LQ, Cao M, Shen J, Chen J. Long non-coding RNA NIFK-AS1 inhibits M2 polarization of macrophages in endometrial cancer through targeting miR-146a. Int J Biochem Cell Biol. 2018; 104:25–33.
https://doi.org/10.1016/j.biocel.2018.08.017
PMID:30176290

35. Shi HZ, Xiong JS, Xu CC, Bu WB, Wang Y, Sun JF, Chen H. Long non-coding RNA expression identified by microarray analysis: Candidate biomarkers in human acral lentiginous melanoma. Oncol Lett. 2020; 19:1465–77.
https://doi.org/10.3892/ol.2019.11207
PMID:31966073

36. Zhou M, Zhang Z, Bao S, Hou P, Yan C, Su J, Sun J. Computational recognition of lncRNA signature of tumor-infiltrating B lymphocytes with potential implications in prognosis and immunotherapy of bladder cancer. Brief Bioinform. 2021; 22:bbaa047.
https://doi.org/10.1093/bib/bbaa047
PMID:32382761

37. Sun M, Geng D, Li S, Chen Z, Zhao W. LncRNA PART1 modulates toll-like receptor pathways to influence

cell proliferation and apoptosis in prostate cancer cells. Biol Chem. 2018; 399:387–95.
https://doi.org/10.1515/hsz-2017-0255
PMID:29261512

38. Liu G, Yuan D, Sun P, Liu W, Wu PF, Liu H, Yu GY. LINC00968 functions as an oncogene in osteosarcoma by activating the PI3K/AKT/mTOR signaling. J Cell Physiol. 2018; 233:8639–47.
https://doi.org/10.1002/jcp.26624
PMID:29904919

39. Wang Y, Zhou J, Xu YJ, Hu HB. Long non-coding RNA LINC00968 acts as oncogene in NSCLC by activating the Wnt signaling pathway. J Cell Physiol. 2018; 233:3397–406.
https://doi.org/10.1002/jcp.26186
PMID:28926089

40. Luan W, Ding Y, Ma S, Ruan H, Wang J, Lu F. Long noncoding RNA LINC00518 acts as a competing endogenous RNA to promote the metastasis of malignant melanoma via miR-204-5p/AP1S2 axis. Cell Death Dis. 2019; 10:855.
https://doi.org/10.1038/s41419-019-2090-3
PMID:31712557

41. Liu Y, Lang T, Zheng Z, Cheng H, Huang X, Wang G, Yin Q, Li Y. In Vivo Environment-Adaptive Nanocomplex with Tumor Cell-Specific Cytotoxicity Enhances T Cells Infiltration and Improves Cancer Therapy. Small. 2019; 15:e1902822.
https://doi.org/10.1002/smll.201902822
PMID:31482673

42. Hartley GP, Chow L, Ammons DT, Wheat WH, Dow SW. Programmed Cell Death Ligand 1 (PD-L1) Signaling Regulates Macrophage Proliferation and Activation. Cancer Immunol Res. 2018; 6:1260–73.
https://doi.org/10.1158/2326-6066.CIR-17-0537
PMID:30012633

43. Liu J, Ding D, Jiang Z, Du T, Liu J, Kong Z. Long non-coding RNA CCAT1/miR-148a/PKCζ prevents cell migration of prostate cancer by altering macrophage polarization. Prostate. 2019; 79:105–12.
https://doi.org/10.1002/pros.23716
PMID:30221381

44. Bucheit AD, Hardy JT, Szender JB, Glitza Oliva IC. Conception and viable twin pregnancy in a patient with metastatic melanoma while treated with CTLA-4 and PD-1 checkpoint inhibition. Melanoma Res. 2020; 30:423–5.
https://doi.org/10.1097/CMR.0000000000000657
PMID:32073510

45. Narahira A, Yanagi T, Kitamura S, Maeda T, Hata H, Asano T, Nozaki A, Kato T, Watari H, Shimizu H. Advanced malignant melanoma successfully treated with dacarbazine following anti-PD-1/CTLA-4 treatment. Int J Dermatol. 2020; 59:e414–6.
https://doi.org/10.1111/ijd.14997
PMID:32496569

46. Seban RD, Moya-Plana A, Antonios L, Yeh R, Marabelle A, Deutsch E, Schwartz LH, Gómez RGH, Saenger Y, Robert C, Ammari S, Dercle L. Prognostic 18F-FDG PET biomarkers in metastatic mucosal and cutaneous melanoma treated with immune checkpoint inhibitors targeting PD-1 and CTLA-4. Eur J Nucl Med Mol Imaging. 2020; 47:2301–12.
https://doi.org/10.1007/s00259-020-04757-3
PMID:32206839

47. Cai J, Qi Q, Qian X, Han J, Zhu X, Zhang Q, Xia R. The role of PD-1/PD-L1 axis and macrophage in the progression and treatment of cancer. J Cancer Res Clin Oncol. 2019; 145:1377–85.
https://doi.org/10.1007/s00432-019-02879-2
PMID:30963235

48. Gordon SR, Maute RL, Dulken BW, Hutter G, George BM, McCracken MN, Gupta R, Tsai JM, Sinha R, Corey D, Ring AM, Connolly AJ, Weissman IL. PD-1 expression by tumour-associated macrophages inhibits phagocytosis and tumour immunity. Nature. 2017; 545:495–9.
https://doi.org/10.1038/nature22396
PMID:28514441

49. Gao J, Shi LZ, Zhao H, Chen J, Xiong L, He Q, Chen T, Roszik J, Bernatchez C, Woodman SE, Chen PL, Hwu P, Allison JP, et al. Loss of IFN-γ Pathway Genes in Tumor Cells as a Mechanism of Resistance to Anti-CTLA-4 Therapy. Cell. 2016; 167:397–404.e9.
https://doi.org/10.1016/j.cell.2016.08.069
PMID:27667683

50. Nennig SE, Schank JR. The Role of NFkB in Drug Addiction: Beyond Inflammation. Alcohol Alcohol. 2017; 52:172–9.
https://doi.org/10.1093/alcalc/agw098
PMID:28043969
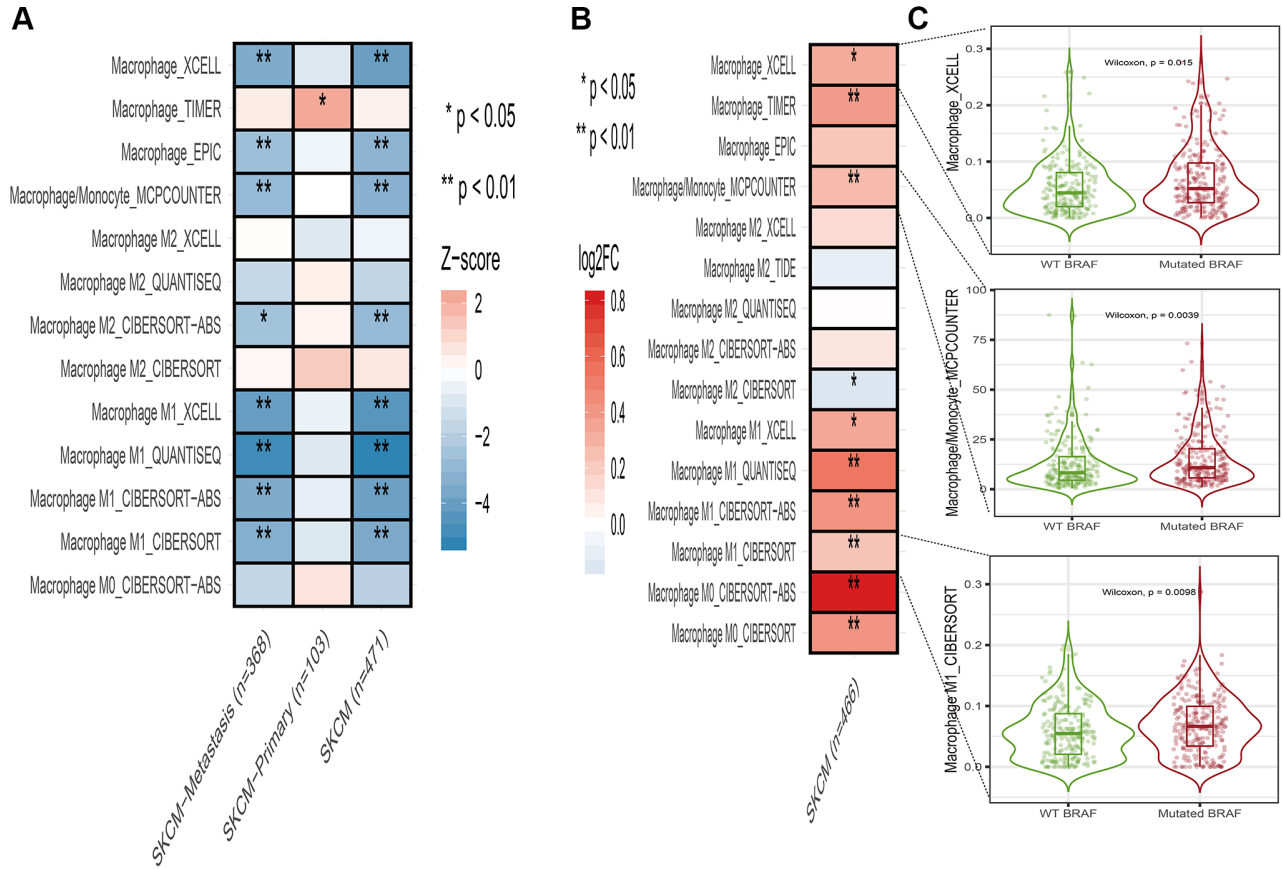
**Supplementary Figure 1. The prognostic value of macrophage in TCGA-SKCM by multiple immune deconvolution methods.** (**A**) Heatmap of multivariable Cox proportional hazard model for macrophage in TCGA-SKCM datasets. (**B**) Heatmap of correlation between macrophage and BRAF mutant. (**C**) Boxplot of macrophage between BRAF mutant and BRAF wildtype.
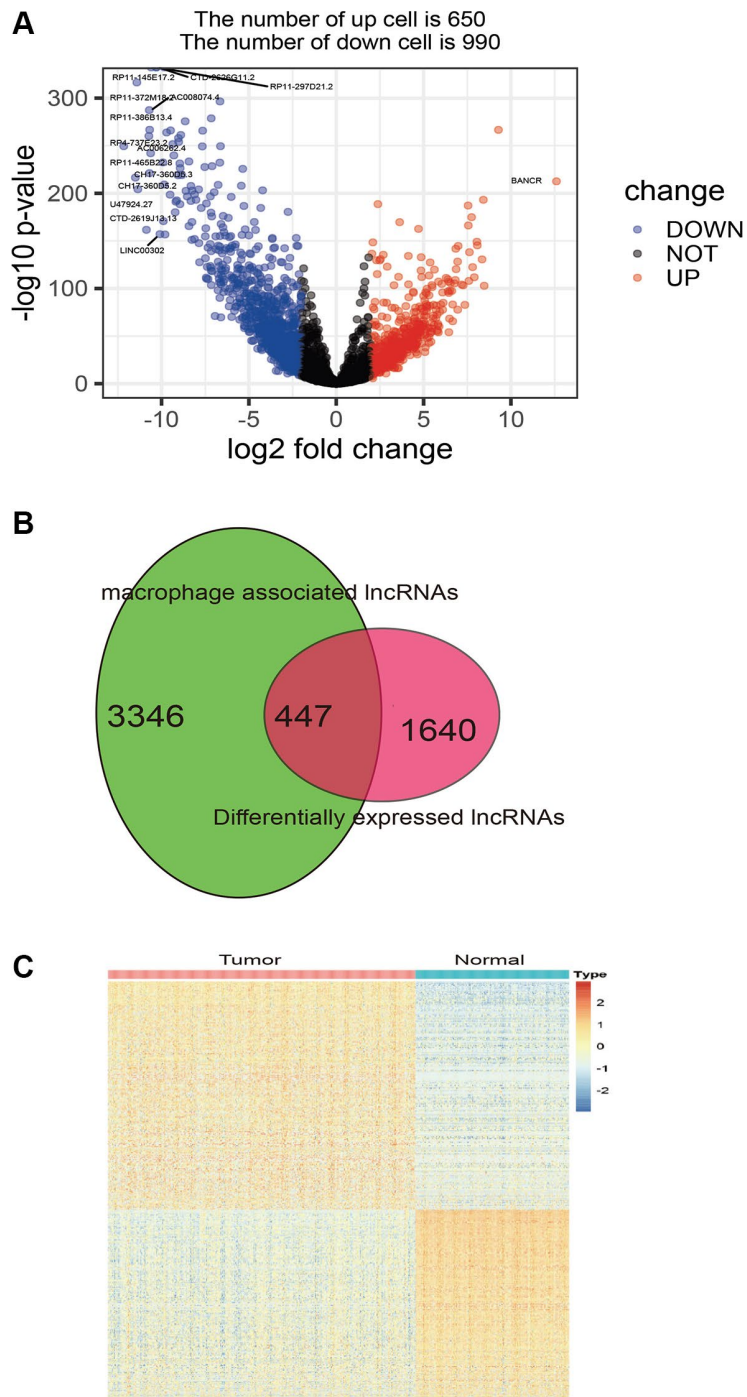
**Supplementary Figure 2. Selection of macrophage associated differentially expressed lncRNAs (DEMlncRNAs).** (**A**) Volcano plot of differentially expressed lncRNAs between normal and melanoma. The highly differentially expressed lncRNAs were labeled (|Log2FC|>10). (**B**) The Venn plot of macrophage associated differentially expressed lncRNAs (DEMlncRNAs). (**C**) Heat map of the DEMlncRNAs in TCGA-SKCM dataset.
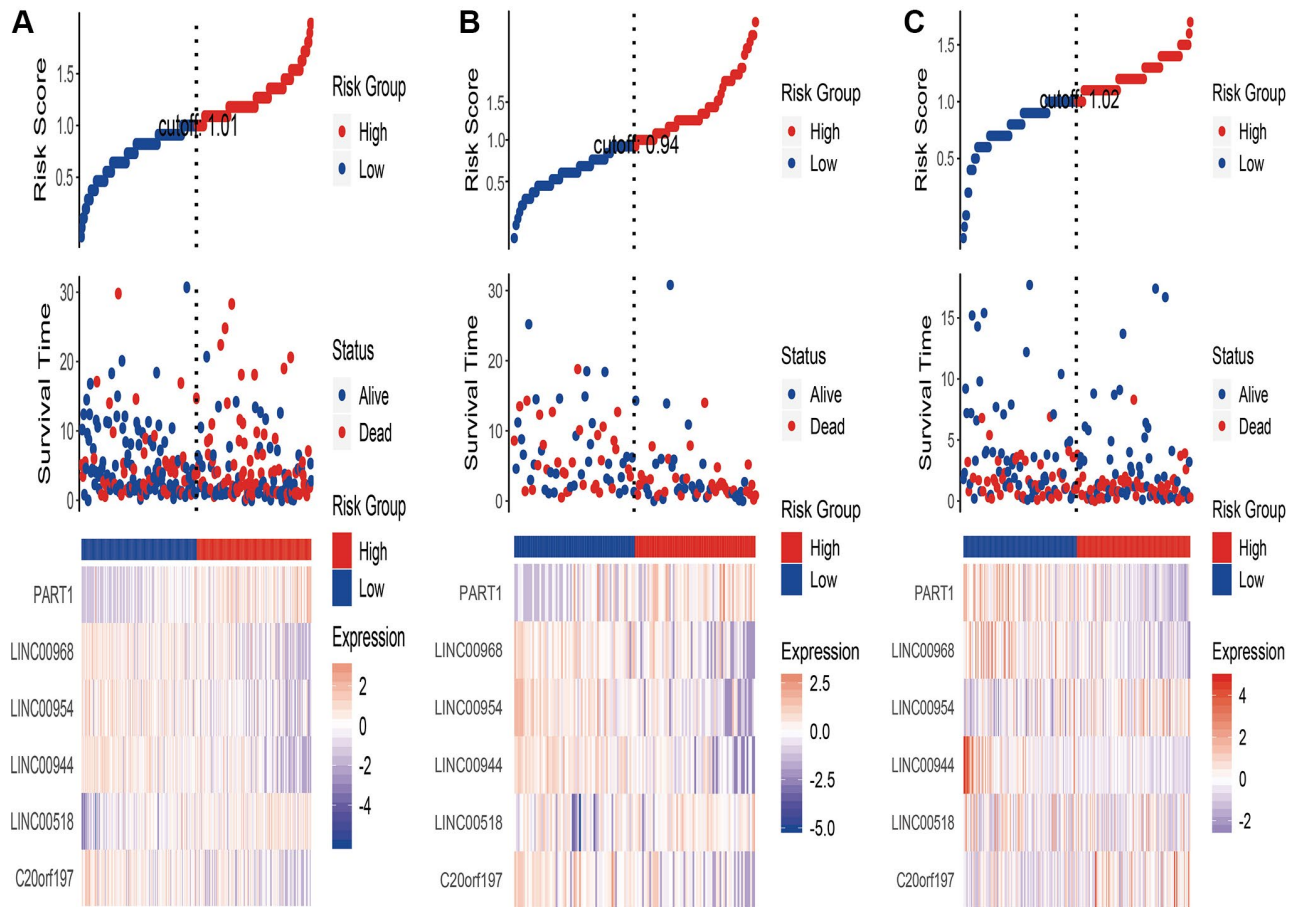
**Supplementary Figure 3. Risk score model.** (**A**) The risk model in train dataset: the distribution of risk score which are arranged in ascending order from left to right; Overall survival (OS) time and life status; The prognostic lncRNA expression patterns. (**B**) The risk model in validation dataset: the distribution of risk score which are arranged in ascending order from left to right; Overall survival (OS) time and life status; The prognostic lncRNA expression patterns. (**C**) The risk model in GSE65904 dataset: the distribution of risk score which are arranged in ascending order from left to right; Overall survival (OS) time and life status; The prognostic lncRNA expression patterns.

## Supplementary Tables

Please browse Full Text version to see the data of Supplementary Tables 1, 2 and 4.


**Supplementary Table 1. The correlation between macrophage and lncRNAs in cutaneous melanoma.**


**Supplementary Table 2. The differentially expressed lncRNAs between tumor and normal groups in TCGA-SKCM&GTEx.**


**Supplementary Table 3. Univariate regression analysis for the six selected DEMlncRNAs.**

| lncRNA_id | lncRNA_symbol | HR | z-value | *p*-value | Lower | Upper |
|---|---|---|---|---|---|---|
| ENSG00000152931 | PART1 | 1.075214 | 2.727958 | 0.006373 | 1.020626 | 1.132721 |
| ENSG00000228784 | LINC00954 | 0.924471 | −2.23804 | 0.025218 | 0.863028 | 0.99029 |
| ENSG00000246430 | LINC00968 | 0.931976 | −2.38642 | 0.017013 | 0.879584 | 0.98749 |
| ENSG00000183674 | LINC00518 | 1.098574 | 2.486129 | 0.012914 | 1.020096 | 1.18309 |
| ENSG00000256128 | LINC00944 | 0.940095 | −2.88669 | 0.003893 | 0.90148 | 0.980364 |
| ENSG00000176659 | C20orf197 | 0.920155 | −2.21562 | 0.026718 | 0.854853 | 0.990444 |


**Supplementary Table 4. The pathway analysis of the six selected DEMlncRNAs.**